HHS Public Access

Author manuscript

*Cell Syst*. Author manuscript; available in PMC 2021 June 24.

Published in final edited form as:

*Cell Syst*. 2020 June 24; 10(6): 515–525.e5. doi:10.1016/j.cels.2020.05.002.

# The scaffold protein Axin promotes signaling specificity within the Wnt pathway by suppressing competing kinase reactions

**Maire Gavagan**[1,2], **Erin Fagnan**[1,2], **Elizabeth B. Speltz**[1], **Jesse G. Zalatan**[1,3,*]

[1]Department of Chemistry, University of Washington, Seattle, WA 98195, USA

[2]These authors contributed equally

[3]Lead Contact

## Summary

Scaffold proteins are thought to promote signaling specificity by accelerating reactions between bound kinase and substrate proteins. To test the long-standing hypothesis that the scaffold protein Axin accelerates GSK3β-mediated phosphorylation of β-catenin in the Wnt signaling network, we measured GSK3β reaction rates with multiple substrates in a minimal, biochemically-reconstituted system. We observed an unexpectedly small, ~2-fold Axin-mediated rate increase for the β-catenin reaction when measured in isolation. In contrast, when both β-catenin and non-Wnt pathway substrates are present, Axin accelerates the β-catenin reaction by preventing competition with alternative substrates. At high competitor concentrations, Axin produces >10-fold rate effects. Thus, while Axin alone does not markedly accelerate the β-catenin reaction, in physiological settings where multiple GSK3β substrates are present, Axin may promote signaling specificity by suppressing interactions with competing, non-Wnt pathway targets. This mechanism for scaffold-mediated control of competition enables a shared kinase to perform distinct functions in multiple signaling networks.

## eTOC blurb

Scaffold proteins are thought to direct signals between alternative outcomes by accelerating reactions between signaling kinases and specific downstream targets. Gavagan, *et al.* use quantitative biochemical reconstitution to demonstrate that the Wnt pathway scaffold protein Axin accomplishes this task by suppressing competing reactions rather than by accelerating one specific reaction.

## Introduction

GSK3β is a central kinase in mammalian cell signaling networks that responds to growth factors and hormones to regulate cell growth, differentiation, and metabolism (Beurel et al.,

*Correspondence: zalatan@uw.edu.

Author contributions

M.G., E.F., E.B.S., and J.G.Z. designed research; M.G., E.F., and E.B.S. performed research; and M.G., E.F., E.B.S., and J.G.Z. wrote the paper.

Declaration of Interests

The authors declare no competing interests.

2015; Kaidanovich-Beilin and Woodgett, 2011). GSK3β receives signals from multiple upstream inputs and acts on several distinct downstream protein targets (Figure 1A). GSK3β-dependent responses to Wnt and growth factor or insulin signals appear to be insulated from each other, so that Wnt signals do not activate alternative GSK3β-dependent pathways and vice versa (Ding et al., 2000; McManus et al., 2005; Ng et al., 2009). These observations raise the fundamental question of how GSK3β activity can be independently regulated by different signaling pathways. Analogous questions arise in many eukaryotic signaling networks, and understanding the mechanisms by which biochemical systems resolve this problem is a major outstanding challenge for the field.

Scaffold proteins that physically assemble protein signaling pathways provide potential mechanisms to direct shared signaling proteins to specific downstream targets (Good et al., 2011; Park et al., 2003; Zalatan et al., 2012). In the Wnt signaling network, the scaffold protein Axin coordinates the assembly of a multi-protein complex including GSK3β and its substrate β-catenin. By binding to both GSK3β and β-catenin, Axin is thought to promote β-catenin phosphorylation (Kimelman and Xu, 2006; MacDonald et al., 2009; Moon et al., 2004; Nusse and Clevers, 2017; Polakis, 2000; Stamos and Weis, 2013). Consequently, regulation of Axin provides a possible mechanism to control GSK3β activity towards β-catenin without affecting GSK3β reactions towards other, non-Wnt pathway substrates (McNeill and Woodgett, 2010).

We know a great deal about the general features of Wnt pathway activation, although the molecular mechanism by which Wnt signaling controls β-catenin phosphorylation and the precise role of Axin in this process is still debated (Nusse and Clevers, 2017). In the absence of a Wnt signal, β-catenin is sequentially phosphorylated by the kinases CK1α and GSK3β, which leads to proteasomal degradation of β-catenin (Figure 1B). Phosphorylation takes place in a multi-protein destruction complex that includes the scaffold protein Axin, the kinases CK1α and GSK3β, the substrate β-catenin, and the accessory proteins Dvl and APC, which may also have scaffolding functions. Wnt pathway activation recruits the destruction complex to the membrane and disrupts its activity, allowing β-catenin to accumulate and activate downstream gene expression. Wnt signaling has been proposed to block β-catenin phosphorylation at both the CK1α and GSK3β kinase reaction steps (Hernandez et al., 2012), possibly via a phosphorylation-dependent conformational change in Axin (S.-E. Kim et al., 2013) or by inhibition of GSK3β when the destruction complex is recruited to the membrane (Stamos et al., 2014).

Initial support for the model that Axin promotes β-catenin phosphorylation came from *in vitro* biochemical experiments showing that the rate of GSK3β-catalyzed β-catenin phosphorylation increases substantially in the presence of Axin (Dajani et al., 2003; Hart et al., 1998; Ikeda et al., 1998). To test this hypothesis, we biochemically reconstituted GSK3β-catalyzed reactions *in vitro* and quantitatively measured reaction rates in the presence and absence of the Axin scaffold protein. By defining a minimal kinetic framework and systematically measuring rate constants for individual reaction steps, we expected to determine whether Axin promotes binding between GSK3β and β-catenin or whether Axin allosterically modulates the activity of a GSK3β•β-catenin complex. Both mechanisms have been observed with other kinase signaling scaffolds (Good et al., 2011), and distinguishing

between these possibilities is an important step towards understanding how Wnt signals might perturb Axin to regulate β-catenin phosphorylation.

Contrary to expectations, we found that Axin has small, ~2-fold effects on the steady state rate constants for β-catenin phosphorylation *in vitro*. We observed similar effects with CK1α-phosphoprimed β-catenin, which is the preferred substrate of GSK3β *in vivo* (Amit et al., 2002; C. Liu et al., 2002), and with unprimed β-catenin, which was used in early biochemical studies (Dajani et al., 2003; Hart et al., 1998; Ikeda et al., 1998). The much larger effects from Axin reported in these earlier studies appear to occur only with unprimed β-catenin under highly specific conditions, and the physiological relevance of these conditions is uncertain. We further demonstrate that Axin has an unexpected ability to suppress GSK3β activity towards other, non-Wnt pathway substrates, and that Axin can produce a >10-fold increase in the β-catenin phosphorylation rate when a competing substrate for GSK3β is present. This effect arises because Axin disrupts binding interactions between GSK3β and its substrates, but rescues the binding defect for one specific substrate by tethering β-catenin to GSK3β. In the cell, where there are >30 substrates of GSK3β (Sutherland, 2011), the ability of Axin to suppress competing reactions provides a mechanism to specifically promote the β-catenin reaction. These findings demonstrate important biochemical features of the Wnt destruction complex and reveal a new model for how scaffold proteins can promote specificity in signaling networks.

## Results

### Reconstituting a minimal destruction complex

To test the model that Axin accelerates the reaction of GSK3β with β-catenin, we biochemically reconstituted a minimal reaction system for quantitative kinetic analysis. We purified recombinant human forms of GSK3β, β-catenin, and Axin as maltose binding protein (MBP) fusions (Figure S1A). We purified active GSK3β from *E. coli* (Q. M. Wang et al., 1994) and found that it was phosphorylated on the activation loop Tyr216 (Figure S1B), as had been previously reported for GSK3β purified from insect cells (Dajani et al., 2003). We purified recombinant primed, phospho-Ser45-β-catenin (pS45-β-catenin) by coexpressing β-catenin with CK1α in *E. coli* (Figure S1C). For comparison, we purified unprimed β-catenin expressed in the absence of CK1α. Finally, we purified full length Axin and a minimal fragment of Axin (miniAxin, residues 384-518) that includes the domains that bind both GSK3β and β-catenin (Dajani et al., 2003; Xing et al., 2003) (Figure S1D).

To confirm that recombinant Axin binds GSK3β and β-catenin in our *in vitro* system, we performed quantitative binding assays using bio-layer interferometry. We determined that full length Axin has a $K_D$ of 7.5 nM for GSK3β. The miniAxin fragment has a $K_D$ of 16 nM for GSK3β (Figure S2A and Table S1). These values are similar to the previously reported $K_D$ of 65 nM for the interaction between human GSK3β and rat Axin (Ikeda et al., 1998). Because miniAxin behaved similarly to full length Axin, and because this construct was easier to express and purify in larger quantity than the full-length protein, we used miniAxin for most subsequent binding and kinetic assays. For several key experiments, we verified that full length Axin demonstrated similar behavior.

We proceeded to measure the affinity of miniAxin for pS45-β-catenin. The observed $K_D$ of 4.0 μM (Figure S2B and Table S1) is similar to the reported $K_D$ of 1.6 μM for unprimed mouse β-catenin binding to a short human Axin fragment (residues 436-498) (Choi et al., 2006). We also attempted to measure an affinity with unprimed β-catenin. We could detect miniAxin binding to unprimed β-catenin in a similar concentration range, but we were unable to accurately measure a $K_D$ value due to surface aggregation artifacts. Taken together, we confirmed that Axin binds to both GSK3β and β-catenin, and that Axin binds GSK3β substantially more tightly than β-catenin.

To determine how Axin affects β-catenin phosphorylation, we measured the steady state rate constants $k_{cat}/K_M$ and $k_{cat}$ in the presence and absence of Axin (Figure 1C). Because Axin binds GSK3β much more tightly than β-catenin, we can define a minimal, simplified kinetic scheme that allows straightforward comparisons. We chose an Axin concentration above the $K_D$ for GSK3β and below the $K_D$ for β-catenin, which ensures that all GSK3β is bound to Axin. Although there is excess free Axin in the system, the concentration of Axin is below the $K_D$ for β-catenin and there should be very little β-catenin bound to free Axin. We obtained steady state rate constants for the Axin•GSK3β complex by varying the β-catenin concentration and compared these values to a reaction of GSK3β with β-catenin in the absence of Axin. If Axin promotes binding between GSK3β and β-catenin, we expect that the observed $K_M$ should shift to a lower concentration and $k_{cat}$ should remain unchanged. Alternatively, if Axin allosterically activates the GSK3β•β-catenin complex, then $k_{cat}$ should increase without necessarily affecting $K_M$. This interpretation potentially oversimplifies the reality of a complex kinetic scheme that could include multiple Axin-bound states, intermediates, and rate-limiting conformational change or product release steps; it nevertheless represents a useful and straightforward starting point.

To measure β-catenin phosphorylation rates, we used quantitative Western blotting. GSK3β sequentially phosphorylates pS45-β-catenin at three sites: T41, S37, and S33 (C. Liu et al., 2002), and product formation can be monitored using an antibody specific for pS33/pS37/pT41-β-catenin (see Methods and Figures S3–S8). This antibody preferentially recognizes the fully phosphorylated β-catenin product over any partially phosphorylated β-catenin intermediates (Figure S3 & S4), and we detected no lag in product formation that would indicate the buildup of partially phosphorylated intermediates in the reaction (Figure S6–S8). We therefore fit the observed rates to a simple Michaelis-Menten kinetic model. In the presence of miniAxin, there is a 1.5-fold increase in the observed value of $k_{cat}$, a 2-fold decrease in the observed value of $K_M$, and a 3-fold increase in $k_{cat}/K_M$ (Figure 1D, Table S2). In the presence of full length Axin, there is a 1.5-fold increase in $k_{cat}$ and no change in $K_M$ within error. These effects are far smaller than expected based on prior reports, one of which suggested that Axin accelerates the reaction by $>10^4$-fold (Dajani et al., 2003; Hart et al., 1998; Ikeda et al., 1998). The conclusion that Axin has a small effect on the β-catenin phosphorylation reaction comes from rates measured at protein concentrations chosen to obtain defined rate constants; we also considered reactions at estimated cellular concentrations and found no effect from Axin (see Box 1 & Figure S9).

When considering the role of Axin in β-catenin phosphorylation, it is important to note that the kinetics could be complicated by the fact that multisite phosphorylation reactions can

proceed through distributive or processive mechanisms. Our observed rates come from detecting pS33/pS37/pT41-β-catenin accumulation (Figure S3 & S4), and we did not measure accumulation of the intermediate phosphorylation states. The observed steady-state kinetic parameters obtained from a Michaelis-Menten model could include contributions from multiple individual phosphorylation steps. Although we did not detect any lag in the initial rate assays which could suggest the buildup of partially phosphorylated intermediates (Figure S7), it is challenging to definitively characterize multisite phosphorylation reactions (Burack and Sturgill, 1997; Ferrell and Bhatt, 1997; Selenko et al., 2008). Further, if β-catenin phosphorylation is distributive, tethering on a scaffold protein could potentially shift the mechanism to processive (Burack and Shaw, 2000). We cannot formally distinguish between these possibilities using the approaches described here. Despite these potential complications, the lack of a large effect from Axin on the observed rate constants for β-catenin phosphorylation remains puzzling.

One possible explanation for the discrepancy between our results and prior work is that scaffold-dependent reactions can be slow if too little scaffold is present, but inhibited at excess scaffold concentrations if the kinase and substrate are not bound to the same scaffold (Levchenko et al., 2000). While we chose an Axin concentration carefully to avoid this issue, it is possible that our assumptions were incorrect. We therefore varied the concentration of miniAxin and measured reaction rates at both saturating and subsaturating pS45-β-catenin concentrations, but found no miniAxin concentration that produced a larger rate enhancement (Figure S10). Thus, Axin has only a modest effect on the GSK3β reaction with pS45-β-catenin, and this effect arises from small changes in $k_{cat}$ and $K_M$. The effect on $K_M$ is relatively small, possibly because Axin binding to β-catenin is weak ($K_D$ ~4 μM) compared to the $K_M$ for the reaction of GSK3β with pS45-β-catenin ($K_M$ = 0.29 μM). In order to obtain large tethering effects from a scaffold, it may be necessary for binding affinities to the scaffold to be at least comparable to the un-scaffolded interaction between kinase and substrate, or for ternary complex formation to be highly cooperative.

## Competition from GSK3β-mediated phosphorylation of Axin does not affect observed rates

Axin can be phosphorylated by GSK3β (S.-E. Kim et al., 2013; Willert et al., 1999), which leads to two potential complicating issues. First, Axin could compete with β-catenin as a substrate for GSK3β, masking any potential rate acceleration mediated by Axin for β-catenin. To test this possibility, we constructed a miniAxin mutant with Ser to Ala substitutions at all four phosphorylation sites (miniAxin-4A), which prevents any detectable phosphorylation by GSK3β (Figure S11A). The miniAxin-4A mutant had small effects on the rate constants for GSK3β-mediated phosphorylation of pS45-β-catenin, indistinguishable from the values observed in reactions with wild type miniAxin (Figure S11B & Table S2). Thus, competition from Axin as a substrate for GSK3β does not appear to affect the observed rates, presumably because at the concentrations in our assay the Axin phosphorylation sites are not saturating the GSK3β active site.

The second potential complication is that phosphorylation of Axin increases its affinity for β-catenin (S.-E. Kim et al., 2013; Willert et al., 1999), which could be necessary to enable Axin to promote β-catenin phosphorylation. Axin phosphorylation promotes β-catenin

binding by relieving an autoinhibitory interaction between the β-catenin binding site and the DIX domain within Axin (S.-E. Kim et al., 2013). Our use of a minimal Axin fragment (miniAxin) was motivated in part to avoid complications from this effect. miniAxin does not include the DIX domain (Figure S1D), so this construct should be fully competent to bind β-catenin. However, regardless of whether the DIX domain was present (full length Axin) or absent (miniAxin), we observed relatively small effects from Axin on GSK3β-mediated phosphorylation of β-catenin (Figure 1D).

## Removing the β-catenin binding site on Axin disrupts the activity of the Axin•GSK3β complex

The Axin•GSK3β complex and free GSK3β have similar $k_{cat}$ and $K_M$ values for β-catenin, suggesting that the β-catenin binding site on Axin should be dispensable. To test this prediction, we removed the β-catenin binding domain (BCD) from Axin (Figure S1D) and assessed the affect of AxinΔBCD on GSK3β activity. Because GSK3β binds to both Axin and AxinΔBCD with similar affinity (Table S1), we can use the same minimal kinetic framework as for wild type Axin (Figure 1C). In the presence of AxinΔBCD, the observed rates for phosphorylation of pS45-β-catenin were substantially slower than the corresponding rates for GSK3β in the absence of Axin (Figure 2), indicating that the activity of the AxinΔBCD•GSK3β complex is suppressed compared to free GSK3β. The reaction does not fully saturate at high pS45-β-catenin concentrations, so we can estimate a conservative limit that $K_M \geq \sim 1$ μM, which is >3-fold larger than the $K_M$ of 0.29 μM in the absence of Axin (Table S2). A simple model to explain this observation is that Axin interferes with the ability of GSK3β to bind substrates. More strictly, this result suggests that Axin interferes with the steady state accumulation of the GSK3β•β-catenin complex or a bound intermediate along the reaction pathway; our discussion below will refer to $K_M$ effects as binding effects, but the analysis holds if the true effect is on steady state accumulation of an intermediate.

The available literature provides some support for the idea that Axin binding can perturb GSK3β activity. A minimal Axin peptide that binds GSK3β has been reported to inhibit GSK3β activity towards multiple substrates, including β-catenin (Zhang et al., 2003). The available crystal structures of GSK3β bound to Axin do not provide a clear explanation for this behavior. Axin does not physically occlude the substrate binding site of GSK3β, and there are no obvious structural changes in the active site between GSK3β bound to Axin and free GSK3β (Dajani et al., 2003; 2001; Stamos et al., 2014). However, the structures were obtained with a 19 amino acid Axin peptide. The minimal fragment reported to inhibit GSK3β was 25 amino acids, and a longer Axin peptide could potentially extend towards the active site. Thus, although we lack a complete structural model, the kinetic data strongly suggest that Axin binding to GSK3β disrupts substrate binding. This detrimental effect is rescued by Axin binding to β-catenin, which restores $K_M$ to its original value. We initially concluded that the lack of an effect on $K_M$ implied that Axin makes no contribution to β-catenin binding to the Axin•GSK3β complex. However, if we compare Axin•GSK3β to AxinΔBCD•GSK3β, there is a ≥4-fold decrease in $K_M$ (Table S2), suggesting that the β-catenin binding domain on Axin does play a role in promoting β-catenin binding to GSK3β.

### Axin slows the GSK3β reaction with non-Wnt pathway substrates

If Axin has two competing functions, disrupting GSK3β substrate binding and promoting binding to β-catenin, we predicted that Axin should have a detrimental effect on the activity of GSK3β with alternative, non-Wnt pathway substrates that do not bind Axin. To determine how Axin affects interactions with these substrates, we measured reaction rates with two non-Wnt pathway substrates, glycogen synthase (GS) and CREB. GS is the canonical substrate of GSK3β in the insulin signaling pathway (Beurel et al., 2015; Kaidanovich-Beilin and Woodgett, 2011). Insulin represses GSK3β but does not activate the Wnt pathway (Ding et al., 2000; McManus et al., 2005; Ng et al., 2009). CREB is a transcription factor that is phosphorylated by GSK3β and integrates signals from a number of pathways (Fiol et al., 1994; Shaywitz and Greenberg, 1999). In cells, PI3K/Akt signaling represses GSK3β, which affects CREB-dependent transcription but does not activate Wnt outputs (Ng et al., 2009; Tullai et al., 2007).

We expressed full length CREB and a short CREB peptide ($CREB_{127\text{-}135}$) as MBP fusions. CREB is phosphorylated by PKA at Ser133, which serves as a priming site for GSK3β to phosphorylate Ser129 (Fiol et al., 1994) (Figure 3A). We phosphorylated both CREB and $CREB_{127\text{-}135}$ to completion *in vitro* with PKA to produce pS133-CREB and pS133-$CREB_{127\text{-}135}$ (Figure S12) and measured reaction rates for GSK3β–catalyzed phosphorylation of pS133-$CREB_{127\text{-}135}$. As predicted, Axin substantially decreased CREB phosphorylation rates (Figure 3B, C, S13, & S14). Axin decreased $k_{cat}/K_M$ by factors of 13-fold for pS133-CREB and 23-fold for pS133-$CREB_{127\text{-}135}$, relative to the same reaction in the absence of Axin (Table S2). The reactions did not detectably saturate in the presence of Axin, suggesting that the $K_M$ has shifted to a much larger value and that at least some of the decrease in $k_{cat}/K_M$ arises from a disruption of binding interactions between GSK3β and pS133-CREB. An alternative possibility is that Axin binds directly to CREB and prevents it from binding GSK3β, but there are no reports of CREB binding to Axin and we did not detect any binding in a pulldown assay (Figure S13).

We also expressed a GS peptide ($GS_{634\text{-}666}$) as an MBP fusion. GS is phosphorylated by CK2 at Ser657 and then sequentially phosphorylated at S653, S649, S645, and S641 by GSK3β (Fiol et al., 1987; 1990) (Figure 3A). We phosphorylated $GS_{634\text{-}666}$ on S657 to completion *in vitro* with CK2 to produce pS657-$GS_{634\text{-}666}$ (Figure S12) and measured reaction rates for GSK3β–catalyzed phosphorylation of pS657-$GS_{634\text{-}666}$ using an antibody specific for pS641 (Figure 3D, S13, & S14). As with β-catenin, multi-site phosphorylation of GS has the potential to be quite mechanistically complicated. Nevertheless, the initial rates for pS641 accumulation were linear and could be fit to a simple Michaelis-Menten model to obtain observed steady state kinetic parameters. Similar to the reaction with CREB, Axin decreased $k_{cat}/K_M$ for pS657-$GS_{634\text{-}666}$ phosphorylation by a factor of 46-fold. Again, the reaction did not detectably saturate in the presence of Axin.

Taken together, these results are consistent with a model where Axin binding inhibits GSK3β activity by increasing the $K_M$ of GSK3β for its substrates and preventing accumulation of GSK3β•substrate complexes. For the reaction with β-catenin, Axin compensates for this inhibition by binding directly to β-catenin and stabilizing the GSK3β•β-catenin complex. Consistent with this model, an Axin mutant that cannot bind to

β-catenin (AxinΔBCD) increases the $K_M$ for the reaction by ≥4-fold (Figure 2 & Table S2). In reactions with the non-Wnt pathway substrates CREB and GS, Axin does not compensate for GSK3β inhibition because it has no native binding interactions to these substrates. Thus, Axin increases the $K_M$ of GSK3β for CREB and GS and substantially decreases the phosphorylation rate at low substrate concentrations below the $K_M$.

## Axin accelerates the β-catenin reaction when competing substrates are present

The Axin-mediated inhibition of GSK3β activity for non-Wnt pathway substrates has a large effect on the specificity of GSK3β for alternative substrates, which can result in large effects on β-catenin phosphorylation rates. Because Axin decreases the $k_{cat}/K_M$ of GSK3β ~10-50-fold for non-Wnt pathway substrates (Figure 3) and increases the $k_{cat}/K_M$ of GSK3β for pS45-β-catenin 3-fold (Figure 1D), the Axin•GSK3β complex is ~$10^2$-fold more specific towards β-catenin than free GSK3β (Figure S15). When both β-catenin and an alternative GSK3β substrate are present at low, subsaturating concentrations, this specificity increase from Axin will manifest largely as a decrease in the rate for the alternative substrate reaction. However, when the non-Wnt pathway substrate is present at saturating concentrations and in excess over β-catenin, Axin can produce larger rate increases for β-catenin phosphorylation. This effect arises because any other GSK3β substrate can act as a competitive inhibitor of the β-catenin reaction. When Axin is added to the system, the $K_M$ for the competitor will increase, resulting in more GSK3β available to react with β-catenin and increasing the rate of β-catenin phosphorylation (Figure 4A & Figure S16). To test this prediction, we measured pS45-β-catenin phosphorylation in a competitive reaction with excess, saturating pS133-$CREB_{127\text{-}135}$ present. In this system, adding Axin produced a 20-fold increase in pS45-β-catenin phosphorylation, much larger than the 3-fold increase in the absence of competitor (Figure 4B). As predicted, this larger effect results entirely from a decrease in the β-catenin phosphorylation rate in the absence of Axin. In the presence of Axin, the β-catenin phosphorylation rates are similar in the presence or absence of competitor because Axin suppresses the competition effect. In the absence of Axin, pS133-$CREB_{127\text{-}135}$ competes for GSK3β and inhibits the β-catenin reaction. We observed a similar effect in the presence of pS657-$GS_{634\text{-}666}$ (Figure 4B), although slightly smaller than with CREB because GS does not fully saturate GSK3β in the reaction conditions tested (Figure S16C). Thus, while Axin alone has a modest effect on the β-catenin reaction rate, in the presence of competing substrates Axin can produce much larger increases in β-catenin phosphorylation. This competition-mediated scaffold effect may be relevant *in vivo*, where GSK3β has many potential competing substrates (Sutherland, 2011) (Figure S16D).

## An inactive GSK3β•β-catenin complex accumulates in the reaction with unprimed β-catenin

Our quantitative kinetic data described above suggest a new model for how the destruction complex specifically accelerates the β-catenin reaction, but a major question remains unanswered: if Axin has only ~2-fold effects on $k_{cat}$ and $K_M$ values for β-catenin phosphorylation, why did early biochemical studies in this system observe much larger rate increases? One notable difference is that the initial biochemical studies on Axin were performed with unprimed β-catenin as a substrate (Dajani et al., 2003; Hart et al., 1998; Ikeda et al., 1998), prior to or concurrent with the discovery of phosphopriming by CK1 (Amit et al., 2002; C. Liu et al., 2002). An early mechanistic model for Axin suggested that

its function might be to bypass the need for phosphopriming (Frame et al., 2001). In this case, either phosphopriming of β-catenin or Axin-mediated tethering would promote the reaction of GSK3β with β-catenin, but there might not be an additional effect from Axin when β-catenin is phosphoprimed. When we measured reaction rates with unprimed β-catenin, we found that the unprimed reaction was ~$10^2$-fold slower than the primed reaction, as expected. However, the steady state rate constants for unprimed β-catenin were not affected by the presence of Axin (Figure S18 & Table S2).

Additional experiments with unprimed β-catenin revealed an unexpected behavior that can explain previous reports of large Axin-mediated rate enhancements. In most circumstances, enzymatic reaction rates should increase linearly with increasing enzyme concentration, and this behavior occurs in the reactions with pS45-β-catenin, pS133-CREB, pS133-$CREB_{127\text{-}135}$, and pS657-$GS_{634\text{-}666}$ (Figure S19). However, when we varied the GSK3β concentration in reactions with unprimed β-catenin, we observed that the rate does not increase linearly with GSK3β concentration. Instead, in the absence of Axin the observed rates level off sharply above ~100 nM GSK3β. In contrast, in the presence of Axin the observed rates increase linearly with GSK3β concentration (Figure S20). This concentration-dependent inactivation of GSK3β could be due to the formation of an inactive dimer or oligomer, and Axin binding to GSK3β could prevent the formation of this inactive state. Thus, if reaction rates are measured at relatively high levels of GSK3β and with unprimed β-catenin, which was the case in the early biochemical studies (Dajani et al., 2003; Hart et al., 1998; Ikeda et al., 1998), Axin produces a large increase in the observed rates.

Based on the kinetic data, the inactive state could be a reversible, oligomeric GSK3β•β-catenin complex (Figure S20–S21). If the inactive state were a dimer or oligomer of GSK3β alone, we would have expected to see a similar inactivation effect in all GSK3β reactions, but this effect is not observed in reactions with pS45-β-catenin, pS133-CREB, pS133-$CREB_{127\text{-}135}$, or pS657-$GS_{634\text{-}666}$ (Figure S19). Thus, the inactive state likely includes both GSK3β and unprimed β-catenin. Further, kinetic modeling suggests that the inactive state is a higher-order oligomer. The observed rates level off too sharply with increasing GSK3β concentration to fit to a dimer model (Figure S20). The proposed inactive oligomer is consistent with the kinetic data, but we cannot exclude alternative models.

The physiological relevance of an oligomeric, inactive GSK3β•β-catenin complex is uncertain. Cellular GSK3β concentrations estimated from mass spectrometry proteomics datasets (Beck et al., 2011; Itzhak et al., 2016; Nagaraj et al., 2011) vary in the range of ~10-300 nM for human HeLa and U2OS cells (cell volumes from BioNumbers BNID 103725 & 108088 (Milo et al., 2010); see also Box 1). These values are similar to the ~100 nM concentration where we see the active/inactive transition *in vitro*, and additional experiments to determine if an oligomeric GSK3β•β-catenin complex exists *in vivo* could be justified. However, the observation that Axin accelerates the β-catenin reaction *in vitro* was the initial foundation to explain the function of the Wnt pathway destruction complex *in vivo* (Kimelman and Xu, 2006; MacDonald et al., 2009; Moon et al., 2004; Nusse and Clevers, 2017; Polakis, 2000; Stamos and Weis, 2013). Our data suggest that the mechanistic origin of this original observation is only applicable to the specific condition of high GSK3β

concentrations reacting with unprimed β-catenin, which is likely not relevant to the preferred physiological reaction of GSK3β with CK1-phosphoprimed pS45-β-catenin.

## Discussion

To understand how Wnt signals regulate Axin to modulate GSK3β activity, we biochemically reconstituted GSK3β-mediated reactions *in vitro* and attempted to reproduce the long-standing result that Axin substantially accelerates the reaction of GSK3β with β-catenin (Dajani et al., 2003; Hart et al., 1998; Ikeda et al., 1998). Although prior reports suggested large effects as high as $10^4$-fold, we found modest 2- to 3-fold effects from Axin on the rate constants for the phosphorylation reaction (Table S2). Two key features of our work can explain this discrepancy. First, we measured *in vitro* reaction rates with the phosphoprimed form of β-catenin, while most prior work used unprimed β-catenin.[1] A large Axin-dependent rate enhancement can be observed with unprimed β-catenin, but only in the specific condition of high GSK3β concentration, where Axin prevents the formation of an oligomeric, inactive GSK3β•β-catenin complex (Figure S20). Second, we measured well-defined rate constants in the presence and absence of Axin, while previous reports made indirect comparisons between observed rates, leading to the estimate of a $10^4$-fold effect from Axin (Dajani et al., 2003).

The small effect of Axin on GSK3β activity towards β-catenin is the result of two opposing effects. First, Axin binding to GSK3β nonspecifically disrupts substrate binding, as seen in the reactions with GS and CREB in the presence of Axin and with β-catenin in the presence of AxinΔBCD (Figures 2 & 3). Second, Axin has a β-catenin binding site that rescues substrate binding specifically for β-catenin. These opposing effects result in ≤2-fold changes in $K_M$ when comparing the β-catenin reactions of Axin•GSK3β to GSK3β, but a larger >4-fold decrease when comparing Axin•GSK3β to AxinΔBCD•GSK3β. Thus, it is reasonable to view Axin as a tethering scaffold that specifically promotes binding of GSK3β to β-catenin, even though there is no net effect of Axin on $K_M$.

How do we reconcile the finding that Axin has small effects on reaction rates *in vitro* with the vast literature that supports the importance of Axin in Wnt signaling (MacDonald et al., 2009; Nusse and Clevers, 2017; Stamos and Weis, 2013)? We know that Axin has substantial effects on Wnt signaling and vertebrate development (Anvarian et al., 2016; Peterson-Nedry et al., 2008; Zeng et al., 1997), and Axin mutants are associated with cancer (Anastas and Moon, 2013; Satoh et al., 2000). Moreover, the idea that the destruction complex acts to accelerate β-catenin phosphorylation is a cornerstone of functional models for Wnt signaling (S.-E. Kim et al., 2013; Lee et al., 2003). One important point to consider is that we do not have a clear framework to evaluate how large of an *in vitro* effect is necessary to account for phenotypic effects *in vivo*, and a 2-fold increase in reaction rates might actually be physiologically meaningful. In cell culture models, treatment with high levels of Wnt ligand can produce ~5-10-fold increases in total β-catenin levels (Hannoush, 2008; Hernandez et al., 2012), with a corresponding ~5-fold decrease in GSK3β-β-catenin

[1] One study included both CK1 and GSK3β in a reaction with β-catenin in the presence and absence of Axin (Ha et al., 2004). The effect of Axin on the observed rates reported in that work is consistent with the rate constants we observe here

phosphorylation rate (Hernandez et al., 2012). 2-fold changes in β-catenin levels also have detectable effects on transcription *in vivo* (Jacobsen et al., 2016). However, the observation that *in vivo* changes in β-catenin levels and phosphorylation rate can substantially exceed 2-fold suggests that we should be able to identify mechanisms that produce correspondingly larger effects *in vitro*.

While Axin alone does not appear to have a sufficiently large effect on β-catenin phosphorylation *in vitro* to account for *in vivo* observations, additional proteins and components that are present *in vivo* could lead to larger effects. We demonstrate one such possible contribution here: Axin produces large increases in reaction rates when another GSK3β substrate is present at saturating concentrations. The β-catenin reaction with GSK3β is inhibited by the presence of competing substrates, and Axin relieves this inhibition to produce much larger increases in the β-catenin phosphorylation rate than observed in the absence of competition (Figure 4). This effect arises because Axin nonspecifically disrupts GSK3β binding to its substrates while simultaneously binding to β-catenin to maintain this specific interaction with GSK3β. The possibility that this effect occurs *in vivo* does not require large physiological GS or CREB concentrations. In a cellular environment, where >30 competing substrates of GSK3β are present (Sutherland, 2011), many possible non-Wnt pathway substrates could contribute to saturating GSK3β and inhibiting the reaction with β-catenin (Figure S16D). Cellular Axin abundances are 10 to $10^3$-fold lower than GSK3β (Beck et al., 2011; Geiger et al., 2012; Itzhak et al., 2016; Lee et al., 2003; Nagaraj et al., 2011; D. Wang et al., 2019), which means that a small fraction of the total GSK3β could be bound to Axin and preferentially phosphorylate β-catenin at rates much faster than the Axin-independent pool. The precise magnitude of this effect depends on the concentrations of GSK3β, Axin, and the competing GSK3β substrates. The Axin-dependent rate enhancement will also depend on how much GSK3β in the Axin-independent pool is free to phosphorylate β-catenin. Other scaffold and adapter proteins are known to engage GSK3β (Beurel et al., 2015), which could produce multiple distinct subpopulations that each promote a specific GSK3β reaction and suppress competitors. We emphasize that the proposed model is a prediction based on a simplified *in vitro* system, which allows us to evaluate the functional behaviors that are possible for biological molecules (see Box 1). Determining whether this mechanism is operative in cells will require experiments that can modulate competition in an *in vivo* setting.

A model where Axin promotes β-catenin phosphorylation by suppressing competing reactions is consistent with our understanding of Wnt and GSK3β function *in vivo*. Wnt signals that disrupt binding interactions to Axin or perturb the conformation of Axin would be predicted to prevent β-catenin phosphorylation. We would also still predict that Wnt signals do not activate other GSK3β-dependent signaling pathways (Ding et al., 2000; McManus et al., 2005; Ng et al., 2009). A Wnt signal that disrupts the Axin•GSK3β complex and relieves the non-specific inhibition of GSK3β could lead to faster reactions with non-Wnt GSK3β substrates, but since the amount of Axin•GSK3β is small relative to the total amount of GSK3β, the overall change in rates towards alternative substrates is likely to be negligible.

Other components from the Wnt pathway are likely to make additional contributions to reactivity and specificity for β-catenin phosphorylation in the destruction complex, although their precise contributions have not yet been quantified. APC is a particularly intriguing candidate (Figure 1B), as it binds Axin and has multiple binding sites for β-catenin in the low nM affinity range (J. Liu et al., 2006; Xing et al., 2004). By binding tightly to β-catenin, the Axin•APC complex could be more effective than Axin alone at tethering β-catenin to GSK3β (Hinoi et al., 2000; Ji et al., 2018; Kishida et al., 1998), leading to larger rate effects. Post-translational modifications of Axin and the formation of higher-order assemblies could also affect reaction rates (S.-E. Kim et al., 2013; Schaefer et al., 2018). It is possible that the destruction complex also promotes the CK1α-mediated phosphopriming step (Amit et al., 2002; C. Liu et al., 2002), which would increase the GSK3β-mediated β-catenin phosphorylation rate. There are conflicting reports on whether Axin accelerates the CK1α-catalyzed reaction *in vitro* (Amit et al., 2002; Ha et al., 2004; Sobrado et al., 2005), and there is evidence that Wnt signals affect both the CK1α and GSK3β-mediated reactions *in vivo* (Hernandez et al., 2012). Finally, Wnt signals may lead to competition for GSK3β by the co-receptors LRP5/6, which can inhibit activity towards β-catenin (Stamos et al., 2014). An important feature of our work is that we have established a clear and quantitative kinetic framework to evaluate the functional effects of Axin on β-catenin phosphorylation, and we can now introduce additional components to evaluate their functional effects, including other kinases, scaffold proteins, and phosphatases.

In addition to providing new insights into Wnt pathway signaling, our results have broad implications for understanding scaffold protein function. Axin was among the earliest proteins identified as a signaling scaffold (Ikeda et al., 1998), and was initially discussed as a prototypical model for tethering a kinase and substrate together to accelerate a phosphorylation reaction (Pawson and Nash, 2003). There is now an emerging consensus that scaffold proteins can have many functions beyond simply tethering a kinase to its substrate, including allosterically modulating the activity of their target proteins (Good et al., 2011). Here we show that Axin does have a tethering function, but the opposing effect from nonspecifically perturbing GSK3β binding to its substrates results in a modest net effect when the activity of Axin is studied in isolation. The functional advantage from Axin-mediated tethering only emerges in a more complex system with multiple competing substrates, which may more accurately reflect the *in vivo* environment. These insights arose from reconstitution and quantitative kinetic characterization of a minimal biochemical system *in vitro*, which highlighted an apparent discrepancy between *in vitro* and *in vivo* behavior and enabled us to identify a possible solution. Future biochemical studies that introduce additional Wnt pathway and GSK3β-interacting proteins will likely provide further insights and rigorous tests to expand our understanding of complex, interconnected cell signaling networks.

## STAR Methods

### RESOURCE AVAILABILITY

**Lead Contact:** Further information and requests for resources should be directed to and will be fulfilled by the Lead Contact, Jesse Zalatan (zalatan@uw.edu).

**Materials Availability:** Plasmids generated in this study will be deposited to Addgene as expeditiously as responsible conduct allows during the COVID-19 pandemic.

**Data and Code Availability:** All data generated for this manuscript are available upon request. A spreadsheet containing the raw data for each figure is included as a supplemental item with the manuscript.

## EXPERIMENTAL MODEL AND SUBJECT DETAILS

All proteins used in this study were expressed in Rosetta (DE3) pLysS *E. coli* cells.

## METHOD DETAILS

**Protein Expression Constructs—**A complete list of protein expression constructs is provided in Table S5. The human Wnt pathway proteins GSK3β, β-catenin, and Axin (hAxin1 isoform 2, Uniprot O15169-2) were cloned into *E. coli* expression vectors containing an N-terminal maltose binding protein (MBP) and a C-terminal His6 tag. GSK3β was also cloned with an N-terminal GST tag and a C-terminal His6 tag for use in pulldown assays. Human coding sequences were obtained as follows: GSK3β (addgene #14753)(He et al., 1995), β-catenin (addgene #17198, a gift from Randall Moon), and Axin (derived from hAxin1-rLuc, a gift from Randall Moon). β-catenin and Axin point mutants were constructed by assembling PCR fragments. CK1α was cloned with an N-terminal GST tag and a C-terminal His6 tag; the human CK1α sequence was obtained from addgene #92014 (Golden et al., 2017). The coexpression plasmid for β-catenin and CK1α was constructed by inserting the GST-CK1α expression cassette (without the His6 tag) into the MBP-β-catenin-His plasmid. Coexpression cassettes with β-catenin mutants were constructed by replacing wt β-catenin with mutant sequences.

Axin truncation constructs $Axin_{384\text{-}518}$ (miniAxin) and $Axin_{\Delta 465\text{-}518}$ (AxinΔBCD) were cloned as described for full length Axin above. MiniAxin contains binding sites for both GSK3β and β-catenin. The N-terminal boundary was defined based on the crystal structure of GSK3β with an Axin peptide (Dajani et al., 2003) and the C-terminal boundary was defined based on the Pfam annotation of the BCD (PF08833) (El-Gebali et al., 2019). The N-terminal boundary of the BCD (for AxinΔBCD) was also defined from the Pfam annotation.

The GSK3β substrates CREB and glycogen synthase were cloned into *E. coli* expression vectors with N-terminal MBP and C-terminal His6 tags. The human CREB coding sequence was obtained from addgene #82203 (E. Kim et al., 2016). The $CREB_{127\text{-}135}$ peptide ILSRRPSYR was cloned by oligo annealing. The glycogen synthase peptide $GS_{634\text{-}666}$ YRYPRPASVPPSPSLSRHSSPHQSEDEEDPRNG was cloned from HEK293 cell cDNA (a gift from Glenna Foight, obtained using an Aurum Total RNA extraction kit (Bio-Rad #7326820) and iScript Reverse Transcription Supermix (Bio-Rad #1708841)). GS peptide boundaries were chosen to encompass the CK2 and GSK3β phosphorylation sites (Fiol et al., 1987) with an extra 7-10 residues flanking each end.

The catalytic subunit of mouse PKA was expressed from pET15b with an N-terminal His-tag (addgene #14921)(Narayana et al., 1997).

**Protein Expression and Purification—**For quantitative kinetic and binding assays, all Wnt pathway, CREB, GS, and PKA proteins were expressed in Rosetta (DE3) pLysS *E. coli* cells by inducing with 0.5 mM IPTG overnight at 18 °C. Constructs with N-terminal MBP and C-terminal His6 tags (GSK3β, β-catenin, Axin, CREB, and GS) were affinity purified with HisPur Ni-NTA resin (Thermo Scientific) and amylose resin (NEB). CK1α was purified with Ni-NTA resin and glutathione agarose resin (Thermo Scientific). The PKA catalytic subunit was purified on Ni-NTA resin. Purified proteins were dialyzed into 20 mM Tris-HCl pH 8.0, 150 mM NaCl, 10% glycerol, and 2 mM DTT at 4 °C, aliquoted and stored at−80 °C. If necessary, proteins were concentrated using 10000 or 30000 MWCO Amicon Ultra-15 Centrifugal Filter devices at 4 °C, 2000×g. Protein concentrations were determined using a Bradford assay (Thermo Scientific). YopH was expressed in BL21 (DE3) *E. coli* cells and purified as previously described (Seeliger et al., 2005). A coomassie gel showing the purity of the proteins used in this work is shown in Figure S1A.

For quantitative binding assays using bio-layer interferometry (Figure S2), MBP-GSK3β was further purified by size exclusion chromatography using a Superdex 200 Increase 10/300 GL column (GE Healthcare) and used immediately.

For pulldown assays, GST-GSK3β, MBP-Axin, and MBP-AxinΔBCD were purified with Ni-NTA resin and used without further purification (Figure S13). pS133-$CREB_{127-135}$ was purified as described below.

**Quantitative Western Blotting—**Protein samples were run on 4-15% miniProtean TGX gels (Bio-Rad) and transferred to 0.2 μm nitrocellulose membranes (Bio-rad). Membranes were blocked with 50:50 Li-Cor blocking buffer:TBST, incubated with antibodies as described below using either manual washes or a Precision Biosystems BlotCycler, visualized using the Li-Cor Odyssey Imaging System, and analyzed using Image Studio Lite 5.2.5 (Li-Cor).

**Determination of the phosphorylation state of GSK3β Tyr216—**200 nM purified GSK3β was incubated with 12 μM tyrosine phosphatase (YopH) for 0.5, 1, or 4 hrs in PMP buffer (New England Biolabs) [50 mM HEPES pH 7.5, 100 mM NaCl, 2 mM DTT, 0.01% Brij 35] at 25 °C (Figure S1B). The level of Tyr216 phosphorylation was assessed by western blotting using a primary Anti-GSK-3β (pY216) antibody (BD Biosciences #612312) and a secondary IRDye 800CW Donkey Anti-Mouse IgG antibody (Li-Cor #926-32212). Total GSK3β (MBP-tagged) was detected by western blotting using a primary MBP Tag (8G1) antibody (Cell Signaling Technology #2396) and a secondary IRDye 800CW Donkey Anti-Mouse IgG antibody (Li-Cor #926-32212).

**Preparation of phospho-primed β-catenin (pS45-β-catenin)—**For quantitative kinetic and binding assays, pS45-β-catenin was obtained by co-expression with CK1α in *E. coli* and purified as described above for β-catenin.

pS45-β-catenin could also be obtained by *in vitro* phosphorylation of β-catenin with purified CK1α. The phosphorylation reaction was performed in a 5 mL volume with 5 μM β-catenin, 1 μM CK1α, and 500 μM ATP in 40 mM HEPES pH 7.4, 50 mM NaCl, 10 mM $MgCl_2$,

0.05% IGEPAL. The reaction was incubated at 25 °C for 1.5 hours (Figure S1C). Kinetic data obtained with this preparation of pS45-β-catenin support the same conclusions as for pS45-β-catenin obtained from co-expression (Figure S8 & S17, Table S3).

For both co-expressed and *in vitro* phosphorylated pS45-β-catenin, the extent of pS45 phosphorylation was evaluated by western blotting using a primary anti-phospho-β-Catenin (Ser45) antibody (Cell Signaling Technology #9564) and a secondary IRDye 800CW Goat Anti-Rabbit IgG antibody (Li-Cor #926-32211).

**Preparation of pS133-CREB, pS133-CREB$_{127-135}$, and pS657-GS$_{634-666}$—***In vitro* phosphorylation reactions of CREB and CREB$_{127-135}$ at Ser133 and of GS$_{634-666}$ at pS657 were performed after Ni-NTA purification. To determine the time necessary for preparative-scale phosphorylation reactions, analytical-scale reactions were performed using $\gamma$–$^{32}$P-ATP (Perkin Elmer #BLU002A). CREB reactions were performed with 10 μM CREB or CREB$_{127-135}$ and 2 μM PKA in 40 mM HEPES pH 7.4, 50 mM NaCl, 10 mM $MgCl_2$, 0.05% IGEPAL, 100 μM unlabeled ATP, and 0.01 μCi/μL $\gamma$–$^{32}$P-ATP at room temperature (21 ± 1 °C). The GS reaction was performed with 5 μM GS$_{634-666}$ and 5 U/μL CK2 (NEB catalog #P6010) in the same reaction conditions except with 0.02 μCi/μL $\gamma$–$^{32}$P-ATP. Reactions were initiated by adding ATP. Timepoints were collected by taking 4.5 μL aliquots, spotting on 0.2 μm nitrocellulose membranes (Bio-rad) and immediately placing the membrane in 0.5% v/v phosphoric acid. Membranes were washed 4X 5 min in 0.5% v/v phosphoric acid, allowed to air dry, exposed to a phosphorimager cassette, and imaged on a GE Typhoon FLA 9000. Images were analyzed using ImageQuant 5.1 (GE Healthcare). The data indicate that the CREB phosphorylation reactions approached completion within the first minute and the GS reaction approached completion within ~200 minutes (Figure S12).

$^{32}$P counts were normalized to concentration using a 1 μM endpoint standard from a reaction of PKA with Kemptide substrate (Adams and Taylor, 1993). Endpoint reactions contained 200 nM PKA, 1 μM MBP-Kemptide, 40 mM Tris pH 7.4, 100 μM EGTA, 10 mM $MgCl_2$, 0.05% IGEPAL, 100 μM unlabeled ATP, and the same amount of $\gamma$–$^{32}$P-ATP as the CREB or GS reaction run in parallel (either 0.01 or 0.02 μCi/μL). Endpoint reactions were incubated for 45 minutes. The Kemptide reaction goes to completion in <1 min (Adams and Taylor, 1993; Speltz and Zalatan, 2020).

Preparative scale phosphorylation of CREB was performed in a 2 mL reaction with 10 μM CREB and 2 μM PKA. Preparative scale phosphorylation of CREB$_{127-135}$ was performed in a 10 mL reaction with 13 μM CREB$_{127-135}$ and 6.5 μM PKA. Preparative scale phosphorylation of GS$_{634-666}$ was performed in a 2 mL reaction with 5 μM GS$_{634-666}$ and 5 U/μL CK2. All reactions had 100 μM ATP in 40 mM HEPES pH 7.4, 50 mM NaCl, 10 mM $MgCl_2$, 0.05% IGEPAL at 25 °C. CREB reactions were incubated for 20 minutes. The GS reaction was incubated for 4 hours. Phosphorylated proteins were purified with amylose resin, concentrated in storage buffer [20 mM Tris-HCl pH 8.0, 150 mM NaCl, 10% glycerol, and 2 mM DTT], aliquoted and stored at-80 °C.

**Quantitative Kinetic Assays—***In vitro* kinetic assays were conducted in kinase assay buffer [40 mM HEPES pH 7.4, 50 mM NaCl, 10 mM $MgCl_2$, and 0.05% IGEPAL] at 25 °C

in 60 μL total volume. Reactions were initiated by adding ATP to a final concentration of 100 μM (this concentration of ATP is saturating for GSK3β–see Figure S5). Reaction timepoints for initial rate kinetics were obtained at 10, 30, 60, and 90 seconds (pS45-β-catenin reactions); 2, 5, 10, and 20 minutes (unprimed β-catenin reactions); 2, 5, 10, and 15 minutes (vary [pS133-CREB] reactions and pS133-CREB vary [GSK3β] reactions with Axin); 0.5, 1, 2, and 5 minutes (pS133-CREB reactions varying [GSK3β] without Axin); 0.5, 1, 2, and 3 minutes (pS133-$CREB_{127-135}$ reactions at [GSK3β] > 20 nM); 2, 5, 10, and 15 minutes (pS133-$CREB_{127-135}$ reactions at [GSK3β] = 20 nM); 5, 10, 20, and 40 minutes (pS657-$GS_{634-666}$ reactions). 10 μL aliquots were quenched by boiling in 5X SDS loading buffer. Samples were analyzed by SDS-PAGE and quantitative western blotting as described above. For reactions with [β-catenin] ≥ 500 nM, gel samples were diluted 2-fold (unprimed β-catenin reactions) or 5-fold (pS45-β-catenin reactions) to prevent a gel smearing artifact.

GSK3β-phosphorylated β-catenin was detected using a primary anti-Phospho-β-Catenin (Ser33/37/Thr41) antibody (Cell Signaling Technology #9561) (Figure S3). GSK3β-phosphorylated CREB was detected using a primary anti-Phospho-CREB (Ser129) antibody (Thermo Scientific PA5-36843) (Figure S13). GSK3β-phosphorylated GS was detected using a primary anti-phospho-GS antibody (Cell Signaling Technology #3891) that recognizes phospho-S641 (Figure S13). For all reactions, the secondary antibody was IRDye 800CW Goat Anti-Rabbit IgG antibody (Li-Cor #926-32211).

Concentrations of phosphorylated β-catenin product were determined by comparing western blot signal intensities to an endpoint standard containing 50 nM β-catenin phosphorylated to completion with GSK3β (Figures S3 and S4). The standard was prepared in a reaction with 50 nM unprimed β-catenin, 100 nM GSK3β, 100 nM miniAxin, and 100 μM ATP in kinase assay buffer at 25 °C for 17 hrs, or in a reaction with 50 nM pS45-β-catenin, 100 nM GSK3β, 100 nM miniAxin, and 100 μM ATP in kinase assay buffer at 25 °C for 25 min. The signal intensities for endpoints prepared from unprimed and phosphoprimed β-catenin were indistinguishable, and adding additional GSK3β and ATP after reaching the endpoint did not further increase the signal (Figure S4). We note that it remains possible that the endpoint standard has not proceeded to 100% completion. The most critical aspect of the endpoint standard is that it allows comparison between reactions analyzed on different gels. If the endpoint standard has not reached 100% completion, the absolute values of the observed rate constants would be smaller than the values reported in Table S2. However, the changes between values for reactions in the presence and absence of Axin would not be affected.

Concentrations of phosphorylated CREB and $CREB_{127-135}$ products were determined with endpoint standards containing 50 nM pS133-CREB or pS133-$CREB_{127-135}$ phosphorylated to completion with GSK3β (Figure S13). The full length CREB standard was prepared in a reaction with 100 nM GSK3β and 100 μM ATP in kinase assay buffer at 25 °C for 3 hours. The $CREB_{127-135}$ standard was prepared in a reaction with 500 nM GSK3β, 100 °M ATP in kinase assay buffer at 25 °C for 2.5 hrs.

Concentrations of phosphorylated $GS_{634-666}$ product were determined with endpoint standards containing 50 nM pS657-$GS_{634-666}$ phosphorylated to completion with GSK3β

(Figure S13). A reaction with 100 nM GSK3β and 100 μM ATP was incubated in kinase assay buffer at 25 μC for 5 hours.

Kinetic parameters were determined by fitting plots of initial rates ($V_{obs}$) vs. [substrate] to the Michaelis-Menten equation $V_{obs} = k_{cat}[E]_0[S]/(K_M + [S])$. Standard errors for $k_{cat}$ and $K_M$ reported in Table S2 are from non-linear least squares fits to this equation. Standard errors for $k_{cat}/K_M$ were obtained by fitting an alternative form of the equation $V_{obs} = (k_{cat}/K_M)[E]_0[S]/(1 + ([S]/K_M))$; errors for $k_{cat}/K_M$ obtained by propagating the errors for $k_{cat}$ and $K_M$ are not accurate in cases where $k_{cat}/K_M$ is well-determined but $K_M$ has a large error because the reaction did not fully saturate over the concentration range tested. For the CREB and GS reactions in the presence of Axin, which did not detectably saturate, the values of $k_{cat}/K_M$ were obtained from the slopes of linear fit to the plots of $V_{obs}$ vs. [substrate]. For the inactive GSK3β oligomer model (Figure S20), the data were fit to the equation: $[GSK3\beta]_{total} = (V_{obs}/k_{cat}) + \left(\left(N/K_{oligomer}\right) \times (V_{obs}/k_{cat})^N\right)$.

**Quantitative Binding Assays—**Binding affinities ($K_D$) and the corresponding association and dissociation rate constants ($k_a$ and $k_d$) were determined with bio-layer interferometry using an Octet Red96e system (ForteBio) and Streptavidin biosensor tips (ForteBio 18-5019). Proteins were biotinylated using an EZ-Link Micro NHS-PEG4-Biotinylation kit (Thermo Scientific 21955) with a molar coupling ratio of 1:1 and purified using 7K MWCO Zeba Spin Desalting Columns (Thermo Scientific). Binding assays were performed in 10 mM $Na_2HPO_4/NaH_2PO_4$ pH 7.4, 137 mM NaCl, 2.6 mM KCl, 0.1% BSA, and 0.02% Tween-20 at 22 °C with Greiner Bio-One 96-Well Non-treated Polypropylene Microplates (Fisher Scientific) at a shake speed of 1000 rpm. Well volumes were 200 μL. Background buffer effects were corrected using a buffer reference sample (a tip loaded with biotinylated protein and dipped into buffer instead of analyte). The buffer reference sample was subtracted from the binding assay data before analysis. Data were analyzed using Data Analysis HT 11.0 (ForteBio) to obtain values of $K_D$, $k_a$ and $k_d$.

For the binding interaction between GSK3β and miniAxin, the miniAxin protein was biotinylated. Biosensor tips were hydrated for 10 minutes in assay buffer, equilibrated for 1 minute, and then loaded with 10 nM biotinylated miniAxin for 5 minutes. After a 1 minute equilibration in assay buffer, tips were immersed in varying concentrations of GSK3β (500 nM, 250 nM, 125 nM, 62.5 nM, 31.3 nM, 15.6 nM, and 7.81 nM) for 5 minutes to monitor association kinetics. Tips were then immersed in assay buffer for 10 minutes to measure dissociation kinetics.

For the binding interaction between pS45-β-catenin and miniAxin, pS45-β-catenin was biotinylated. Biosensor tips were hydrated for 10 minutes in assay buffer, equilibrated for 1 minute, and then loaded with 30 nM nM biotinylated pS45-β-catenin for 5 minutes. Tips were sequentially washed 3X for 1 minute in assay buffer to minimize a baseline drift effect that occurred if these wash steps were omitted. Tips were immersed in varying concentrations of miniAxin (10 μM, 2.5 μM, 625 nM, 156.25 nM) for 100 seconds to monitor association kinetics. Tips were then immersed in assay buffer for 60 seconds to measure dissociation kinetics.

**Pulldown binding assays—**Pulldown binding assays with GST-GSK3β and MBP-tagged Axin and pS133-CREB$_{127\text{-}135}$ were performed in 60 μL total volumes with 3 μM GST-GSK3β bait, 6 μM target proteins, and 20 μL of 50% glutathione agarose resin slurry (Thermo Scientific) in kinase assay buffer [40 mM HEPES pH 7.4, 50 mM NaCl, 10 mM $MgCl_2$, and 0.05% IGEPAL]. Binding reactions were incubated at 4 °C for 1.5 hr. The resin was pelleted (1 min, 100×g) and washed 5X with 200 μL buffer. Samples were eluted by boiling in 1X SDS loading buffer for 10 minutes and analyzed by SDS PAGE (Figure S13).

**Phos-tag gel analysis of Axin phosphorylation state—**Phos-tag gels were prepared with 10% acrylamide, 25 μM phos-tag acrylamide, and 50 μM $MnCl_2$ with a 4.5% acrylamide stacking gel, stained with SYPRO Ruby (Thermo Scientific S12000), and imaged on a GE Typhoon FLA 9000.

### QUANTIFICATION AND STATISTICAL ANALYSIS

Phosphorylated protein levels from quantitative western blots were analyzed using Image Studio Lite 5.2.5 (Li-Cor). Phosphorylated protein levels from $\gamma$–$^{32}$P-ATP reactions were analyzed using ImageQuant 5.1 (GE Healthcare).

Kinetic parameters for phosphorylation reactions were determined by fitting to kinetic models as described above using the curve fit function of Kaleidagraph 4.1.3. Standard errors for $k_{cat}$, $K_M$, and $k_{cat}/K_M$ are from non-linear least squares fits to the initial rate data (Table S2). Initial rate measurements were performed in triplicate.

Binding affinities ($K_D$) and the corresponding association and dissociation rate constants ($k_a$ and $k_d$) from bio-layer interferometry experiments were obtained using Data Analysis HT 11.0 (ForteBio) (Table S1). Binding constants, rate constants, and their associated standard errors are obtained from global fits to at least four independent binding assays (Figure S2).

## Supplementary Material

Refer to Web version on PubMed Central for supplementary material.

## Acknowledgements

We thank Dustin Maly, Dan Herschlag, John Scott, Jonathan Cooper, David Kimelman, Wendell Lim, Michael Gelb, Steven Wiley, Geeta Narlikar, Wenqing Xu, Renée van Amerongen, Edmond Fischer, and members of the Zalatan group for comments and discussion. We thank Sujata Chakraborty for purifying YopH and Glenna Foight for providing human cDNA. This work was supported by a Career Award at the Scientific Interface from the Burroughs Wellcome Fund (J.G.Z.) and NIH R35 GM124773 (J.G.Z.).

## References

Adams JA, Taylor SS, 1993. Phosphorylation of peptide substrates for the catalytic subunit of cAMP-dependent protein kinase. J. Biol. Chem. 268, 7747–7752. [PubMed: 8463304]

Amit S, Hatzubai A, Birman Y, Andersen JS, Ben-Shushan E, Mann M, Ben-Neriah Y, Alkalay I, 2002. Axin-mediated CKI phosphorylation of β-catenin at Ser 45: a molecular switch for the Wnt pathway. Genes Dev. 16, 1066–1076. doi:10.1101/gad.230302 [PubMed: 12000790]

Anastas JN, Moon RT, 2013. WNT signalling pathways as therapeutic targets in cancer. Nat. Rev. Cancer 13, 11–26. doi:10.1038/nrc3419 [PubMed: 23258168]

Anvarian Z, Nojima H, van Kappel EC, Madl T, Spit M, Viertler M, Jordens I, Low TY, van Scherpenzeel RC, Kuper I, Richter K, Heck AJR, Boelens R, Vincent J-P, Rüdiger SGD, Maurice MM, 2016. Axin cancer mutants form nanoaggregates to rewire the Wnt signaling network. Nat. Struct. Mol. Biol. 23, 324–332. doi:10.1038/nsmb.3191 [PubMed: 26974125]

Beck M, Schmidt A, Malmstroem J, Claassen M, Ori A, Szymborska A, Herzog F, Rinner O, Ellenberg J, Aebersold R, 2011. The quantitative proteome of a human cell line. Mol. Syst. Biol. 7, 549. doi:10.1038/msb.2011.82 [PubMed: 22068332]

Beurel E, Grieco SF, Jope RS, 2015. Glycogen synthase kinase-3 (GSK3): regulation, actions, and diseases. Pharmacol. Ther. 148, 114–131. doi:10.1016/j.pharmthera.2014.11.016 [PubMed: 25435019]

Burack WR, Shaw AS, 2000. Signal transduction: hanging on a scaffold. Curr. Opin. Cell Biol. 12, 211–216. [PubMed: 10712921]

Burack WR, Sturgill TW, 1997. The activating dual phosphorylation of MAPK by MEK is nonprocessive. Biochemistry 36, 5929–5933. doi:10.1021/bi970535d [PubMed: 9166761]

Choi H-J, Huber AH, Weis WI, 2006. Thermodynamics of β-catenin-ligand interactions: the roles of the N-and C-terminal tails in modulating binding affinity. J. Biol. Chem. 281, 1027–1038. doi:10.1074/jbc.M511338200 [PubMed: 16293619]

Dajani R, Fraser E, Roe SM, Yeo M, Good VM, Thompson V, Dale TC, Pearl LH, 2003. Structural basis for recruitment of glycogen synthase kinase 3β to the axin-APC scaffold complex. EMBO J. 22, 494–501. doi:10.1093/emboj/cdg068 [PubMed: 12554650]

Dajani R, Fraser E, Roe SM, Young N, Good V, Dale TC, Pearl LH, 2001. Crystal structure of glycogen synthase kinase 3β: structural basis for phosphate-primed substrate specificity and autoinhibition. Cell 105, 721–732. doi:10.1016/s0092-8674(01)00374-9 [PubMed: 11440715]

Ding VW, Chen RH, McCormick F, 2000. Differential regulation of glycogen synthase kinase 3β by insulin and Wnt signaling. J. Biol. Chem. 275, 32475–32481. doi:10.1074/jbc.M005342200 [PubMed: 10913153]

El-Gebali S, Mistry J, Bateman A, Eddy SR, Luciani A, Potter SC, Qureshi M, Richardson LJ, Salazar GA, Smart A, Sonnhammer ELL, Hirsh L, Paladin L, Piovesan D, Tosatto SCE, Finn RD, 2019. The Pfam protein families database in 2019. Nucleic Acids Res. 47, D427–D432. doi:10.1093/nar/gky995 [PubMed: 30357350]

Ferrell JE, Bhatt RR, 1997. Mechanistic studies of the dual phosphorylation of mitogen-activated protein kinase. J. Biol. Chem. 272, 19008–19016. doi:10.1074/jbc.272.30.19008 [PubMed: 9228083]

Fersht AR, 1999. Structure and Mechanism in Protein Science. W.H. Freeman and Company.

Fiol CJ, Mahrenholz AM, Wang Y, Roeske RW, Roach PJ, 1987. Formation of protein kinase recognition sites by covalent modification of the substrate. Molecular mechanism for the synergistic action of casein kinase II and glycogen synthase kinase 3. J. Biol. Chem. 262, 14042–14048. [PubMed: 2820993]

Fiol CJ, Wang A, Roeske RW, Roach PJ, 1990. Ordered multisite protein phosphorylation. Analysis of glycogen synthase kinase 3 action using model peptide substrates. J. Biol. Chem. 265, 6061–6065. [PubMed: 2156841]

Fiol CJ, Williams JS, Chou CH, Wang QM, Roach PJ, Andrisani OM, 1994. A secondary phosphorylation of $CREB^{341}$ at $Ser^{129}$ is required for the cAMP-mediated control of gene expression. A role for glycogen synthase kinase-3 in the control of gene expression. J. Biol. Chem. 269, 32187–32193. [PubMed: 7798217]

Frame S, Cohen P, Biondi RM, 2001. A common phosphate binding site explains the unique substrate specificity of GSK3 and its inactivation by phosphorylation. Mol. Cell 7, 1321–1327. doi:10.1016/S1097-2765(01)00253-2 [PubMed: 11430833]

Fraser E, Young N, Dajani R, Franca-Koh J, Ryves J, Williams RSB, Yeo M, Webster M-T, Richardson C, Smalley MJ, Pearl LH, Harwood A, Dale TC, 2002. Identification of the Axin and Frat binding region of Glycogen Synthase Kinase-3. J. Biol. Chem. 277, 2176–2185. doi:10.1074/jbc.M109462200 [PubMed: 11707456]

Geiger T, Wehner A, Schaab C, Cox J, Mann M, 2012. Comparative proteomic analysis of eleven common cell lines reveals ubiquitous but varying expression of most proteins. Mol Cell Proteomics 11, M111.014050. doi:10.1074/mcp.M111.014050

Golden RJ, Chen B, Li T, Braun J, Manjunath H, Chen X, Wu J, Schmid V, Chang T-C, Kopp F, Ramirez-Martinez A, Tagliabracci VS, Chen ZJ, Xie Y, Mendell JT, 2017. An Argonaute phosphorylation cycle promotes microRNA-mediated silencing. Nature 542, 197–202. doi:10.1038/nature21025 [PubMed: 28114302]

Good M, Tang G, Singleton J, Reményi A, Lim WA, 2009. The Ste5 scaffold directs mating signaling by catalytically unlocking the Fus3 MAP kinase for activation. Cell 136, 1085–1097. doi:10.1016/j.cell.2009.01.049 [PubMed: 19303851]

Good MC, Zalatan JG, Lim WA, 2011. Scaffold proteins: hubs for controlling the flow of cellular information. Science 332, 680–686. doi:10.1126/science.1198701 [PubMed: 21551057]

Ha N-C, Tonozuka T, Stamos JL, Choi H-J, Weis WI, 2004. Mechanism of phosphorylation-dependent binding of APC to β-catenin and its role in β-catenin degradation. Mol. Cell 15, 511–521. doi:10.1016/j.molcel.2004.08.010 [PubMed: 15327768]

Hannoush RN, 2008. Kinetics of Wnt-driven β-catenin stabilization revealed by quantitative and temporal imaging. PLoS ONE 3, e3498. doi:10.1371/journal.pone.0003498 [PubMed: 18941539]

Hart MJ, de los Santos R, Albert IN, Rubinfeld B, Polakis P, 1998. Downregulation of β-catenin by human Axin and its association with the APC tumor suppressor, β-catenin and GSK3β. Curr. Biol. 8, 573–581. [PubMed: 9601641]

He X, Saint-Jeannet JP, Woodgett JR, Varmus HE, Dawid IB, 1995. Glycogen synthase kinase-3 and dorsoventral patterning in *Xenopus* embryos. Nature 374, 617–622. doi:10.1038/374617a0 [PubMed: 7715701]

Hernandez AR, Klein AM, Kirschner MW, 2012. Kinetic responses of β-catenin specify the sites of Wnt control. Science 338, 1337–1340. doi:10.1126/science.1228734 [PubMed: 23138978]

Hinoi T, Yamamoto H, Kishida M, Takada S, Kishida S, Kikuchi A, 2000. Complex formation of adenomatous polyposis coli gene product and axin facilitates glycogen synthase kinase-3β-dependent phosphorylation of β-catenin and down-regulates β-catenin. J. Biol. Chem. 275, 34399–34406. doi:10.1074/jbc.M003997200 [PubMed: 10906131]

Ikeda S, Kishida S, Yamamoto H, Murai H, Koyama S, Kikuchi A, 1998. Axin, a negative regulator of the Wnt signaling pathway, forms a complex with GSK-3β and β-catenin and promotes GSK-3β-dependent phosphorylation of β-catenin. EMBO J. 17, 1371–1384. doi:10.1093/emboj/17.5.1371 [PubMed: 9482734]

Itzhak DN, Tyanova S, Cox J, Borner GH, 2016. Global, quantitative and dynamic mapping of protein subcellular localization. eLife 5, e16950. doi:10.7554/eLife.16950 [PubMed: 27278775]

Jacobsen A, Heijmans N, Verkaar F, Smit MJ, Heringa J, van Amerongen R, Feenstra KA, 2016. Construction and experimental validation of a Petri net model of Wnt/β-Catenin signaling. PLoS ONE 11, e0155743. doi:10.1371/journal.pone.0155743 [PubMed: 27218469]

Ji L, Lu B, Wang Z, Yang Z, Reece-Hoyes J, Russ C, Xu W, Cong F, 2018. Identification of ICAT as an APC inhibitor, revealing Wnt-dependent inhibition of APC-Axin interaction. Mol. Cell 72, 37–47.e4. doi:10.1016/j.molcel.2018.07.040 [PubMed: 30197296]

Kaidanovich-Beilin O, Woodgett JR, 2011. GSK-3: Functional insights from cell biology and animal models. Front. Mol. Neurosci. 4, 40. doi:10.3389/fnmol.2011.00040 [PubMed: 22110425]

Kim E, Ilic N, Shrestha Y, Zou L, Kamburov A, Zhu C, Yang X, Lubonja R, Tran N, Nguyen C, Lawrence MS, Piccioni F, Bagul M, Doench JG, Chouinard CR, Wu X, Hogstrom L, Natoli T, Tamayo P, Horn H, Corsello SM, Lage K, Root DE, Subramanian A, Golub TR, Getz G, Boehm JS, Hahn WC, 2016. Systematic Functional Interrogation of Rare Cancer Variants Identifies Oncogenic Alleles. Cancer Discov 6, 714–726. doi:10.1158/2159-8290.CD-16-0160 [PubMed: 27147599]

Kim S-E, Huang H, Zhao M, Zhang X, Zhang A, Semonov MV, MacDonald BT, Zhang X, Garcia Abreu J, Peng L, He X, 2013. Wnt stabilization of β-catenin reveals principles for morphogen receptor-scaffold assemblies. Science 340, 867–870. doi:10.1126/science.1232389 [PubMed: 23579495]

Kimelman D, Xu W, 2006. β-catenin destruction complex: insights and questions from a structural perspective. Oncogene 25, 7482–7491. doi:10.1038/sj.onc.1210055 [PubMed: 17143292]

Kishida S, Yamamoto H, Ikeda S, Kishida M, Sakamoto I, Koyama S, Kikuchi A, 1998. Axin, a negative regulator of the Wnt signaling pathway, directly interacts with adenomatous polyposis coli and regulates the stabilization of β-catenin. J. Biol. Chem. 273, 10823–10826. doi:10.1074/jbc.273.18.10823 [PubMed: 9556553]

Lee E, Salic A, Krüger R, Heinrich R, Kirschner MW, 2003. The roles of APC and Axin derived from experimental and theoretical analysis of the Wnt pathway. PLoS Biol. 1, E10. doi:10.1371/journal.pbio.0000010 [PubMed: 14551908]

Levchenko A, Bruck J, Sternberg PW, 2000. Scaffold proteins may biphasically affect the levels of mitogen-activated protein kinase signaling and reduce its threshold properties. Proc. Natl. Acad. Sci. USA 97, 5818–5823. doi:10.1073/pnas.97.11.5818 [PubMed: 10823939]

Liu C, Li Y, Semenov M, Han C, Baeg GH, Tan Y, Zhang Z, Lin X, He X, 2002. Control of β-catenin phosphorylation/degradation by a dual-kinase mechanism. Cell 108, 837–847. doi:10.1016/s0092-8674(02)00685-2 [PubMed: 11955436]

Liu J, Xing Y, Hinds TR, Zheng J, Xu W, 2006. The third 20 amino acid repeat is the tightest binding site of APC for β-catenin. J. Mol. Biol. 360, 133–144. doi:10.1016/j.jmb.2006.04.064 [PubMed: 16753179]

MacDonald BT, Tamai K, He X, 2009. Wnt/β-catenin signaling: components, mechanisms, and diseases. Dev. Cell 17, 9–26. doi:10.1016/j.devcel.2009.06.016 [PubMed: 19619488]

McManus EJ, Sakamoto K, Armit LJ, Ronaldson L, Shpiro N, Marquez R, Alessi DR, 2005. Role that phosphorylation of GSK3 plays in insulin and Wnt signalling defined by knockin analysis. EMBO J. 24, 1571–1583. doi:10.1038/sj.emboj.7600633 [PubMed: 15791206]

McNeill H, Woodgett JR, 2010. When pathways collide: collaboration and connivance among signalling proteins in development. Nat. Rev. Mol. Cell Biol. 11, 404–413. doi:10.1038/nrm2902 [PubMed: 20461097]

Milo R, Jorgensen P, Moran U, Weber G, Springer M, 2010. BioNumbers-the database of key numbers in molecular and cell biology. Nucleic Acids Res. 38, D750–3. doi:10.1093/nar/gkp889 [PubMed: 19854939]

Moon RT, Kohn AD, De Ferrari GV, Kaykas A, 2004. WNT and β-catenin signalling: diseases and therapies. Nat. Rev. Genet. 5, 691–701. doi:10.1038/nrg1427 [PubMed: 15372092]

Nagaraj N, Wisniewski JR, Geiger T, Cox J, Kircher M, Kelso J, Pääbo S, Mann M, 2011. Deep proteome and transcriptome mapping of a human cancer cell line. Mol. Syst. Biol. 7, 548. doi:10.1038/msb.2011.81 [PubMed: 22068331]

Narayana N, Cox S, Shaltiel S, Taylor SS, Xuong N, 1997. Crystal structure of a polyhistidine-tagged recombinant catalytic subunit of cAMP-dependent protein kinase complexed with the peptide inhibitor PKI(5–24) and adenosine. Biochemistry 36, 4438–4448. doi:10.1021/bi961947 [PubMed: 9109651]

Ng SS, Mahmoudi T, Danenberg E, Bejaoui I, de Lau W, Korswagen HC, Schutte M, Clevers H, 2009. Phosphatidylinositol 3-kinase signaling does not activate the Wnt cascade. J. Biol. Chem. 284, 35308–35313. doi:10.1074/jbc.M109.078261 [PubMed: 19850932]

Nusse R, Clevers H, 2017. Wnt/β-Catenin Signaling, Disease, and Emerging Therapeutic Modalities. Cell 169, 985–999. doi:10.1016/j.cell.2017.05.016 [PubMed: 28575679]

Park S-H, Zarrinpar A, Lim WA, 2003. Rewiring MAP kinase pathways using alternative scaffold assembly mechanisms. Science 299, 1061–1064. doi:10.1126/science.1076979 [PubMed: 12511654]

Pawson T, Nash P, 2003. Assembly of cell regulatory systems through protein interaction domains. Science 300, 445–452. doi:10.1126/science.1083653 [PubMed: 12702867]

Peterson-Nedry W, Erdeniz N, Kremer S, Yu J, Baig-Lewis S, Wehrli M, 2008. Unexpectedly robust assembly of the Axin destruction complex regulates Wnt/Wg signaling in Drosophila as revealed by analysis in vivo. Dev. Biol. 320, 226–241. doi:10.1016/j.ydbio.2008.05.521 [PubMed: 18561909]

Polakis P, 2000. Wnt signaling and cancer. Genes Dev. 14, 1837–1851. [PubMed: 10921899]

Satoh S, Daigo Y, Furukawa Y, Kato T, Miwa N, Nishiwaki T, Kawasoe T, Ishiguro H, Fujita M, Tokino T, Sasaki Y, Imaoka S, Murata M, Shimano T, Yamaoka Y, Nakamura Y, 2000. AXIN1 mutations in hepatocellular carcinomas, and growth suppression in cancer cells by virus-mediated transfer of AXIN1. Nat. Genet. 24, 245–250. doi:10.1038/73448 [PubMed: 10700176]

Schaefer KN, Bonello TT, Zhang S, Williams CE, Roberts DM, McKay DJ, Peifer M, 2018. Supramolecular assembly of the beta-catenin destruction complex and the effect of Wnt signaling on its localization, molecular size, and activity in vivo. PLoS Genet. 14, e1007339. doi:10.1371/journal.pgen.1007339 [PubMed: 29641560]

Seeliger MA, Young M, Henderson MN, Pellicena P, King DS, Falick AM, Kuriyan J, 2005. High yield bacterial expression of active c-Abl and c-Src tyrosine kinases. Protein Sci 14, 3135–3139. doi:10.1110/ps.051750905 [PubMed: 16260764]

Selenko P, Frueh DP, Elsaesser SJ, Haas W, Gygi SP, Wagner G, 2008. *In situ* observation of protein phosphorylation by high-resolution NMR spectroscopy. Nat. Struct. Mol. Biol. 15, 321–329. doi:10.1038/nsmb.1395 [PubMed: 18297086]

Shaywitz AJ, Greenberg ME, 1999. CREB: a stimulus-induced transcription factor activated by a diverse array of extracellular signals. Annu. Rev. Biochem. 68, 821–861. doi:10.1146/annurev.biochem.68.1.821 [PubMed: 10872467]

Sobrado P, Jedlicki A, Bustos VH, Allende CC, Allende JE, 2005. Basic region of residues 228–231 of protein kinase CK1α is involved in its interaction with Axin: binding to Axin does not affect the kinase activity. J. Cell. Biochem. 94, 217–224. doi:10.1002/jcb.20350 [PubMed: 15565646]

Speltz EB, Zalatan JG, 2020. The relationship between effective molarity and affinity governs rate enhancements in tethered kinase-substrate reactions. bioRxiv. doi:10.1101/2020.03.12.989012

Stamos JL, Chu ML-H, Enos MD, Shah N, Weis WI, 2014. Structural basis of GSK-3 inhibition by N-terminal phosphorylation and by the Wnt receptor LRP6. eLife 3, e01998. doi:10.7554/eLife.01998 [PubMed: 24642411]

Stamos JL, Weis WI, 2013. The β-catenin destruction complex. Cold Spring Harb. Perspect. Biol. 5, a007898. doi:10.1101/cshperspect.a007898 [PubMed: 23169527]

Sutherland C, 2011. What are the *bona fide* GSK3 substrates? Int J Alzheimers Dis 2011, 505607. doi:10.4061/2011/505607 [PubMed: 21629754]

Tullai JW, Chen J, Schaffer ME, Kamenetsky E, Kasif S, Cooper GM, 2007. Glycogen synthase kinase-3 represses cyclic AMP response element-binding protein (CREB)-targeted immediate early genes in quiescent cells. J. Biol. Chem. 282, 9482–9491. doi:10.1074/jbc.M700067200 [PubMed: 17277356]

Wang D, Eraslan B, Wieland T, Hallström B, Hopf T, Zolg DP, Zecha J, Asplund A, Li L-H, Meng C, Frejno M, Schmidt T, Schnatbaum K, Wilhelm M, Ponten F, Uhlén M, Gagneur J, Hahne H, Kuster B, 2019. A deep proteome and transcriptome abundance atlas of 29 healthy human tissues. Mol. Syst. Biol. 15, e8503. doi:10.15252/msb.20188503 [PubMed: 30777892]

Wang QM, Fiol CJ, DePaoli-Roach AA, Roach PJ, 1994. Glycogen synthase kinase-3β is a dual specificity kinase differentially regulated by tyrosine and serine/threonine phosphorylation. J. Biol. Chem. 269, 14566–14574. doi:10.3892/ijo.2015.3135 [PubMed: 7514173]

Willert K, Shibamoto S, Nusse R, 1999. Wnt-induced dephosphorylation of Axin releases β-catenin from the Axin complex. Genes Dev. 13, 1768–1773. doi:10.1101/gad.13.14.1768 [PubMed: 10421629]

Wisniewski JR, Ostasiewicz P, Duś K, Zielińska DF, Gnad F, Mann M, 2012. Extensive quantitative remodeling of the proteome between normal colon tissue and adenocarcinoma. Mol. Syst. Biol. 8, 611. doi:10.1038/msb.2012.44 [PubMed: 22968445]

Xing Y, Clements WK, Kimelman D, Xu W, 2003. Crystal structure of a β-catenin/Axin complex suggests a mechanism for the β-catenin destruction complex. Genes Dev. 17, 2753–2764. doi:10.1101/gad.1142603 [PubMed: 14600025]

Xing Y, Clements WK, Le Trong I, Hinds TR, Stenkamp R, Kimelman D, Xu W, 2004. Crystal structure of a β-catenin/APC complex reveals a critical role for APC phosphorylation in APC function. Mol. Cell 15, 523–533. doi:10.1016/j.molcel.2004.08.001 [PubMed: 15327769]

Zalatan JG, Coyle SM, Rajan S, Sidhu SS, Lim WA, 2012. Conformational control of the Ste5 scaffold protein insulates against MAP kinase misactivation. Science 337, 1218–1222. doi:10.1126/science.1220683 [PubMed: 22878499]

Zeng L, Fagotto F, Zhang T, Hsu W, Vasicek TJ, Perry WL, Lee JJ, Tilghman SM, Gumbiner BM, Costantini F, 1997. The mouse Fused locus encodes Axin, an inhibitor of the Wnt signaling pathway that regulates embryonic axis formation. Cell 90, 181–192. doi:10.1016/s0092-8674(00)80324-4 [PubMed: 9230313]

Zhang F, Phiel CJ, Spece L, Gurvich N, Klein PS, 2003. Inhibitory phosphorylation of glycogen synthase kinase-3 (GSK-3) in response to lithium. Evidence for autoregulation of GSK-3. J. Biol. Chem. 278, 33067–33077. doi:10.1074/jbc.M212635200 [PubMed: 12796505]

**Box 1.**

### The relevance of *in vitro* rate measurements for reactions in cells

A common question posed for biochemical studies is whether rate effects measured *in vitro* are relevant at physiological concentrations in cells. This question is complicated by fundamental limitations in our understanding of cell biology. A seemingly straightforward approach would be to use rate constants measured *in vitro* to predict the effect of the Axin scaffold for any arbitrary set of concentrations, including at estimated cellular concentrations of kinase, substrate, and scaffold. The predictions could then be confirmed by measuring observed rates at these cellular concentrations. We took this approach using concentrations for HeLa, a widely-studied cell line, and colon cells, where Wnt signaling is active. In both cases reliable protein abundance values are available from mass spectrometry data, which can be converted to concentration using cell volumes from microscopy data (Table S4). Using our measured rate constants (Table S2) and the affinity of Axin for GSK3β to estimate the amount of the Axin•GSK3β complex (Table S1), we predict no effect from Axin, and for both cell types the observed rates at these concentrations match the prediction (Figure S9).

Although performing *in vitro* experiments at estimated *in vivo* concentrations is technically straightforward, it is important to recognize that determining *in vivo* concentrations is inherently problematic. The state of the cell, including the cell cycle and external perturbations, will affect measured protein abundances. Competition from other binding partners will also have serious confounding effects. Total protein abundance includes proteins engaged in multiple different complexes or in different post-translationally modified states, which will not reflect the amount of free protein that is available for a particular reaction of interest. Defining a cell volume is equally challenging. Much of the cell is occupied by organelles and other structures, so the actual cell volume may be much smaller than the value obtained from a size-based microscopy measurement. In addition, cells are not well-mixed solutions. Rather, they are spatially heterogeneous with variations in local protein abundance throughout due to localization signals, recruitment to protein complexes, and phase separation effects. Given these challenges, it is difficult to establish the cellular concentrations that should be used to measure and compare observed rates *in vitro*. Instead, we suggest that *in vitro* concentrations should be chosen so that rate constants can be measured, which allows well-defined comparisons to be made between different reaction conditions. The purpose of comparisons in simplified model systems is not to ascertain what is happening inside a cell, but rather to develop a rigorous understanding of what functional behaviors, in principle, are possible in biological systems.

## Highlights

- The Axin scaffold protein directs the kinase GSK3β between alternative substrates
- Axin does not dramatically boost rate constants for GSK3β reacting with β-catenin
- Axin suppresses GSK3β reactions with competing substrates
- When multiple substrates are present, Axin accelerates the β-catenin reaction

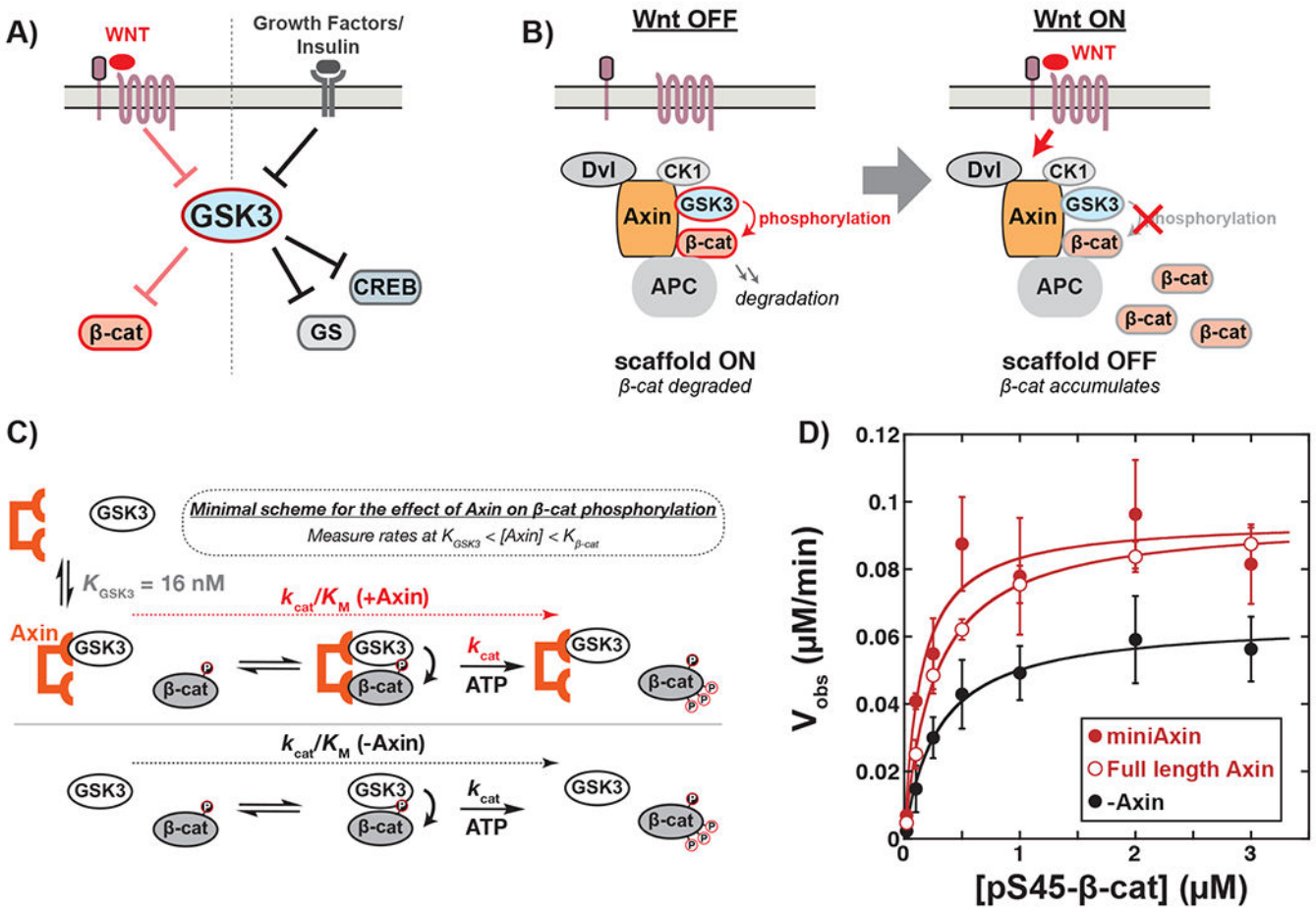


**Figure 1.**

Axin assembles signaling proteins in the Wnt pathway.

(A) GSK3β receives input signals from Wnt, growth factors, and hormones like insulin and acts on multiple distinct downstream targets. (B) GSK3β assembles into a multi-protein destruction complex with β-catenin, CK1α, Axin, Dvl, and APC. In the absence of a Wnt signal, β-catenin is phosphorylated and degraded. In the presence of a Wnt signal, β-catenin phosphorylation is blocked, which allows β-catenin to accumulate. (C) Minimal kinetic scheme for the reaction of GSK3β with pS45-β-catenin in the presence and absence of Axin. GSK3β phosphorylates pS45-β-catenin at three sites: S33, S37, and T41. When $K_{GSK3}$ < [Axin] < $K_{β\text{-}cat}$, all GSK3β is bound to Axin (when [Axin] > [GSK3β]) and there should be very little pS45-β-catenin bound to free Axin. (D) Michaelis-Menten plot of $V_{obs}$ vs. [pS45-β-catenin] at 20 nM GSK3β in the presence and absence of 500 nM miniAxin or full length (FL) Axin. Values are mean ± SD for at least 3 measurements. See Figures S6–S8 for representative western blot images and plots of product vs. time used to obtain the initial rate values ($V_{obs}$) plotted here. See Table S2 for values of fitted kinetic parameters.

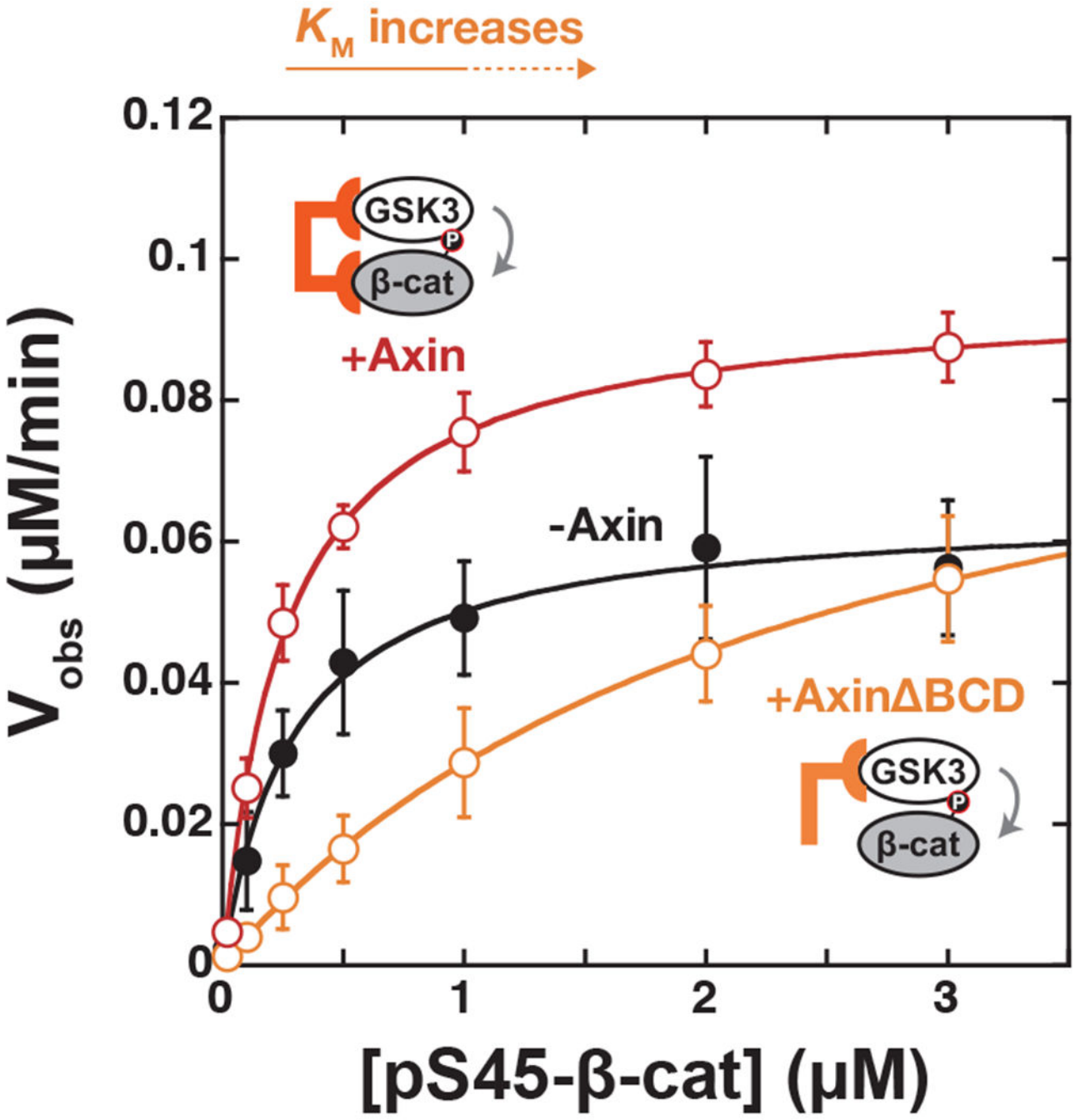


**Figure 2.**

Removing the β-catenin binding site on Axin disrupts the activity of the Axin•GSK3β complex.

Michaelis-Menten plot of $V_{obs}$ vs. [pS45-β-catenin] at 20 nM GSK3β in the presence and absence of 500 nM full length Axin or AxinΔBCD. At low substrate concentrations, the AxinΔBCD reaction is slower than both the Axin reaction and the no Axin reaction. Values are mean ± SD for at least 3 measurements. See Table S2 for values of fitted kinetic parameters. The AxinΔBCD reaction does not fully saturate at high [pS45-β-catenin], which

means that only the value of $k_{cat}/K_M$ can be accurately determined. The reaction may be starting to saturate, suggesting a conservative limit of $K_M \geq \sim 1$ μM.

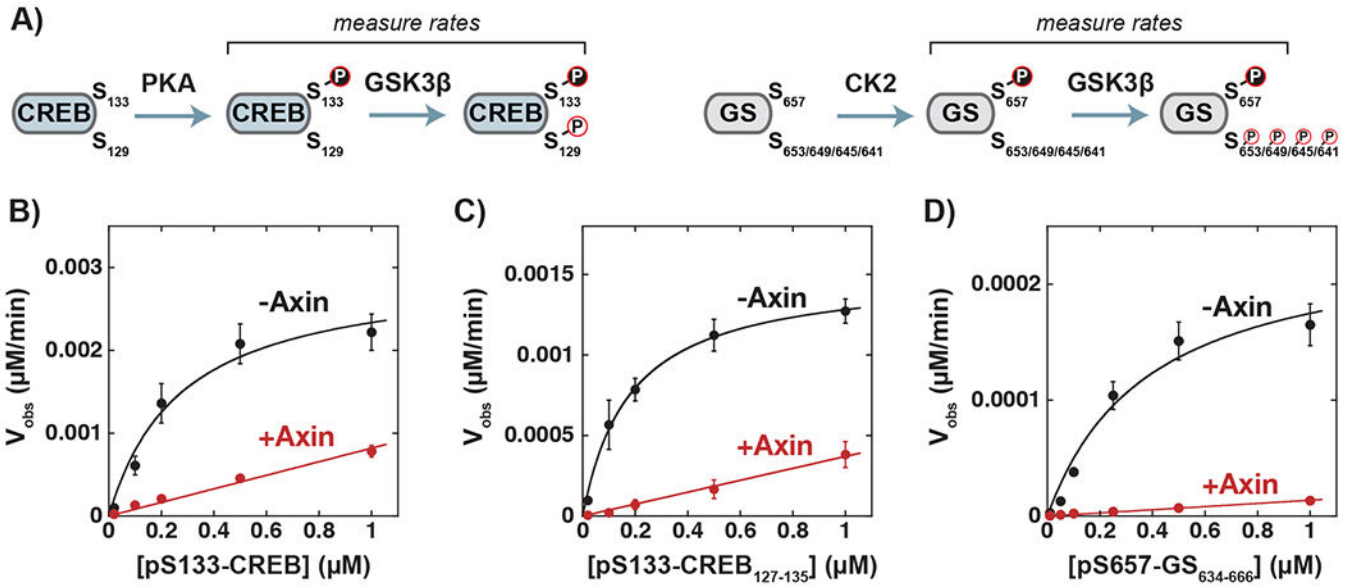


**Figure 3.**

Axin decreases phosphorylation rates of non-Wnt pathway GSK3β substrates.

(A) Minimal schemes for phosphorylation of CREB and GS. PKA phosphorylates CREB at S133. pS133 serves as a priming site for GSK3β, which phosphorylates pS133-CREB at S129. CK2 phosphorylates GS at S657, which primes sequential GSK3β reactions at S653/S649/S645/S641. (B-D) Michaelis-Menten plots of $V_{obs}$ vs. substrate for (B) [pS133-CREB], (C) [pS133-$CREB_{127-135}$], and (D) [pS657-$GS_{634-666}$] at 20 nM GSK3β in the presence and absence of 500 nM miniAxin. Values are mean ± SD for at least 3 measurements. See Table S2 for values of fitted kinetic parameters. There is no detectable saturation of the reactions in the presence of miniAxin up to 1 μM substrate, which means that only the value of $k_{cat}/K_M$ can be determined from the slope of a linear fit to the data. We were unable to detect GSK3β-catalyzed phosphorylation of unprimed $CREB_{127–133}$ ($V_{obs} \leq 3 \times 10^{-5}$ μM/min at 0.5 μM $CREB_{127–133}$) or $GS_{634-666}$ ($V_{obs} \leq 6 \times 10^{-7}$ μM/min at 0.2 μM $GS_{634-666}$).

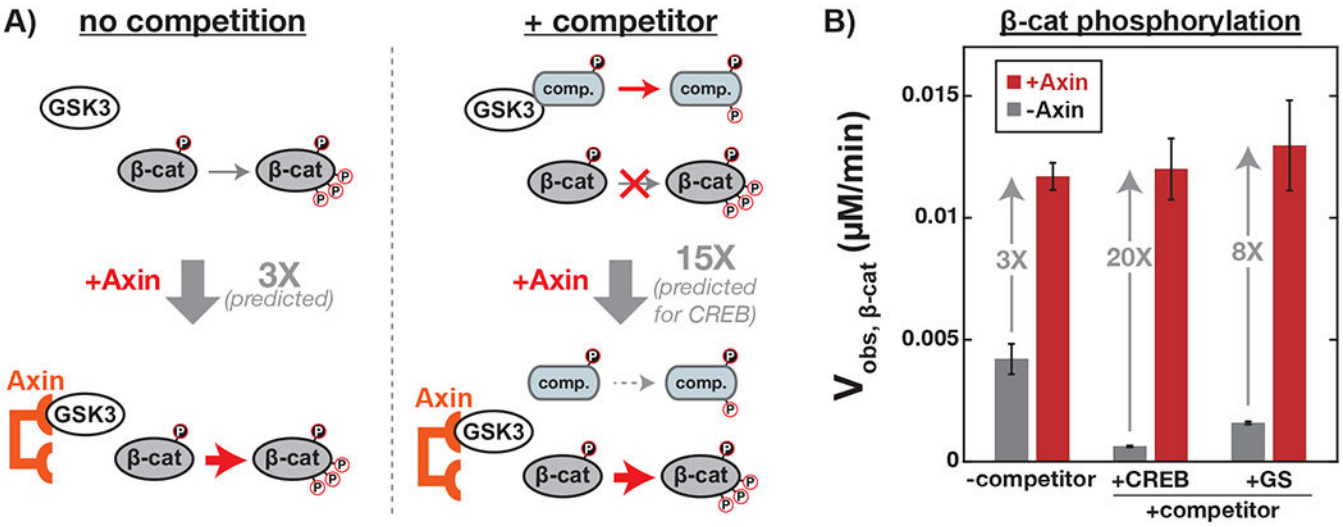


**Figure 4.**

Axin accelerates the β-catenin reaction when competing substrates are present.

(A) Prediction for the effect of Axin on pS45-β-catenin phosphorylation when a competing substrate is present. When a competitor is present at saturating concentrations and pS45-β-catenin is present at subsaturating concentrations, the competitor forms a complex with GSK3β and inhibits the reaction with pS45-β-catenin. Axin disrupts the interaction of GSK3β with the competitor, preventing buildup of the GSK3β•competitor complex. Using a Michaelis-Menten model with a pS133-$CREB_{127\text{-}135}$ competitive inhibitor present at 1 μM concentration (Figure S16B), we predict that Axin should produce a 15-fold increase on the β-catenin phosphorylation rate in the presence of pS133-$CREB_{127\text{-}135}$, much larger than the 3-fold increase in the absence of competitor. A similar analysis with pS657-$GS_{634\text{-}666}$ as the competitor predicts an 8-fold increase in β-catenin (Figure S16C); the predicted effect is smaller than for CREB because the $K_M$ of GSK3β for GS is larger (Table S2) and 1 μM GS is not fully saturating. (B) β-catenin phosphorylation rates ($V_{obs}$) measured at 20 nM GSK3β and 50 nM pS45-β-catenin (subsaturating) in the presence and absence of 500 nM miniAxin with either no competitor, 1 μM pS133-$CREB_{127\text{-}135}$, or 1 μM pS657-$GS_{634\text{-}666}$. Values are mean ± SD for at least 3 measurements. In the absence of competitor, Axin produces a 3-fold rate increase. In the presence of CREB or GS competitors, Axin produces 20-fold or 8-fold rate increases, respectively, similar to the predicted values.

## KEY RESOURCES TABLE

| REAGENT or RESOURCE | SOURCE | IDENTIFIER |
|---|---|---|
| Antibodies | | |
| Anti-GSK-3β (pY216) | BD Biosciences | Cat# 612312; RRID:AB_399627 |
| MBP Tag (8G1) | Cell Signaling Technology | Cat# 2396; RRID:AB_2140060 |
| anti-phospho-β-Catenin (Ser45) | Cell Signaling Technology | Cat# 9564; RRID:AB_331150 |
| anti-Phospho-β-Catenin (Ser33/37/Thr41) | Cell Signaling Technology | Cat# 9561; RRID:AB_331729 |
| anti-Phospho-CREB (Ser129) | Thermo Scientific | Cat# PA5–36843; RRID:AB_2553772 |
| anti-Phospho-Glycogen Synthase (Ser641) | Cell Signaling Technology | Cat# 3891; RRID:AB_2116390 |
| IRDye 800CW Donkey Anti-Mouse IgG | Li-Cor | Cat# #926–32212; RRID:AB_621847 |
| IRDye 800CW Goat Anti-Rabbit IgG | Li-Cor | Cat# 926–32211; RRID:AB_621843 |
| | | |
| Bacterial and Virus Strains | | |
| *E. coli* Rosetta (DE3) pLysS | Fisher Scientific | Cat# 70 956 3 |
| | | |
| | | |
| Biological Samples | | |
| | | |
| | | |
| | | |
| Chemicals, Peptides, and Recombinant Proteins | | |
| Ni-NTA resin | Thermo Scientific | Cat# PI88223 |
| Amylose resin | New England Biolabs | Cat# E8021 |
| Glutathione agarose resin | Thermo Scientific | Cat# PI16101 |
| $\gamma^{-32}$P-ATP 3000Ci/mmol 10 mCi/ml | Perkin-Elmer | Cat# BLU002A |
| Phos-tag Acrylamide AAL-107 | Wako Chemicals | Cat# 304–93521 |
| Casein Kinase II (CK2) | New England Biolabs | Cat# P6010 |
| PageRuler Prestained Protein Ladder, 10 to 180 kDa | Thermo Scientific | Cat# 26616 |
| SYPRO Ruby Protein Gel Stain | Thermo Scientific | Cat# S12000 |
| | | |
| Critical Commercial Assays | | |
| Streptavidin biosensor tips | ForteBio | Cat# 18–5019 |
| EZ-Link Micro NHS-PEG4-Biotinylation kit | Thermo Scientific | Cat# 21955 |
| | | |
| Deposited Data | | |
| | | |
| | | |
| | | |
| Experimental Models: Cell Lines | | |
| | | |
| | | |
| | | |
| Experimental Models: Organisms/Strains | | |
| | | |
| | | |
| | | |
| Oligonucleotides | | |
| | | |
| | | |
| | | |

| REAGENT or RESOURCE | SOURCE | IDENTIFIER |
|---|---|---|
| Recombinant DNA | | |
| pES001 MBP-GSK3β-HA-His | This paper (see Table S3) | N/A |
| pMG033 GST-GSK3β-HA-His | This paper (see Table S3) | N/A |
| pEF073 MBP-Axin-His | This paper (see Table S3) | N/A |
| pMG023 MBP-Axin$_{384–518}$-His | This paper (see Table S3) | N/A |
| pMG031 MBP-Axin$_{384–518}$ T481A/S486A/S493A/S496A -His | This paper (see Table S3) | N/A |
| pMG035 MBP-Axin$_{\Delta465–518}$-His | This paper (see Table S3) | N/A |
| pEF019 MBP-β-catenin-His | This paper (see Table S3) | N/A |
| pMG050 MBP-β-catenin S45A-His | This paper (see Table S3) | N/A |
| pMG047 MBP-β-catenin S33A-His | This paper (see Table S3) | N/A |
| pMG057 MBP-β-catenin S33A/S37A-His | This paper (see Table S3) | N/A |
| pMG061 MBP-β-catenin S33A/S37A/T41A-His | This paper (see Table S3) | N/A |
| pMG062 MBP-β-catenin S33A/S37A/T41A/S45A-His | This paper (see Table S3) | N/A |
| pMG051 MBP-β-catenin-His, GST-CK1α | This paper (see Table S3) | N/A |
| pMG063 MBP-β-catenin S45A-His, GST-CK1α | This paper (see Table S3) | N/A |
| pMG064 MBP-β-catenin S33A-His, GST-CK1α | This paper (see Table S3) | N/A |
| pMG065 MBP-β-catenin S33A/S37A-His, GST-CK1α | This paper (see Table S3) | N/A |
| pMG066 MBP-β-catenin S33A/S37A/T41A-His, GST-CK1α | This paper (see Table S3) | N/A |
| pMG066 MBP-β-catenin S33A/S37A/T41A/S45A-His, GST-CK1α | This paper (see Table S3) | N/A |
| pMG046 GST-CK1α-His | This paper (see Table S3) | N/A |
| pEF086 MBP-CREB$_{127-135}$-His | This paper (see Table S3) | N/A |
| pEF087 MBP-CREB$_{127-135}$ S133A-His | This paper (see Table S3) | N/A |
| pMG059 MBP-CREB-His | This paper (see Table S3) | N/A |
| pMG058 MBP-Glycogen Synthase$_{634-666}$-His | This paper (see Table S3) | N/A |
| $H_6$-rC His-PKA-rC | Addgene | Cat# 14921 |
| pES010 MBP-Kemptide-His | Speltz & Zalatan, 2020 | N/A |
| pCDFDuet-1 YopH | Seeliger et al., 2005 | N/A |

| **REAGENT or RESOURCE** | **SOURCE** | **IDENTIFIER** |
|---|---|---|
| pJZ101 MBP-His | This paper (see Table S3) | N/A |
| pJZ102 GST-His | This paper (see Table S3) | N/A |
| | | |
| Software and Algorithms | | |
| Image Studio Lite 5.2.5 | Li-Cor | |
| ImageQuant 5.1 | GE Healthcare | |
| Kaleidagraph 4.1.3 | Synergy Software | |
| Data Analysis HT 11.0 | ForteBio | |
| | | |
| Other | | |
| | | |
| | | |
| | | |